



12-2015

Installation and Alignment of the N3He Experiment

Eric Lee Plemons

University of Tennessee - Knoxville, eplemons@vols.utk.edu

Recommended Citation

Plemons, Eric Lee, "Installation and Alignment of the N3He Experiment. " Master's Thesis, University of Tennessee, 2015.
https://trace.tennessee.edu/utk_gradthes/3601

This Thesis is brought to you for free and open access by the Graduate School at Trace: Tennessee Research and Creative Exchange. It has been accepted for inclusion in Masters Theses by an authorized administrator of Trace: Tennessee Research and Creative Exchange. For more information, please contact trace@utk.edu.

To the Graduate Council:

I am submitting herewith a thesis written by Eric Lee Plemons entitled "Installation and Alignment of the N3He Experiment." I have examined the final electronic copy of this thesis for form and content and recommend that it be accepted in partial fulfillment of the requirements for the degree of Master of Science, with a major in Physics.

Geoff Greene, Major Professor

We have read this thesis and recommend its acceptance:

Nadia Fomin, Kate Jones

Accepted for the Council:

Carolyn R. Hodges

Vice Provost and Dean of the Graduate School

(Original signatures are on file with official student records.)

Installation and Alignment of the N3He Experiment

A Thesis Presented for the

Master of Science

Degree

The University of Tennessee, Knoxville

Eric Lee Plemons

December 2015

Copyright © 2015 by Eric Lee Plemons

All rights reserved.

ABSTRACT

The $n^3\text{He}$ experiment is designed to probe the hadronic weak interaction by measuring the parity violating asymmetry between the spin of incoming neutrons and the momentum of outgoing protons following the nuclear break up of a helium three upon absorbing a neutron. Cold neutrons from the SNS are first polarized then allowed to impact a target chamber filled with helium three where the reaction occurs. Energetic particles resulting from the nuclear breakup ionize the helium three gas and are thereby detected as currents by an array of signal wires within the target chamber. In order to make a statistics limited measurement on the order of $\pm 10\%$ systematic alignment errors must be carefully controlled. Of greatest importance are the direction and magnitude of the magnetic field within the experiment, location of the neutron beam centroid, and the alignment of the primary components with respect to them. The equipment and methods utilized to achieve these alignments will be discussed as will the results of the alignment procedures.

TABLE OF CONTENTS

CHAPTER 1: THEORY AND MOTIVATION	1
Strong Interaction.....	1
Residual Strong Interaction.....	2
Weak Interaction.....	2
Parity Violation.....	3
Hadronic Weak Force	3
CHAPTER 2: EXPERIMENTAL APPARATUS.....	7
Experimental Overview	7
Neutron Production	8
Frame Definition Choppers.....	8
Supermirror Polarizer	9
Resonant Frequency Spin Rotator.....	9
Magnetic Holding Field	10
Magnetic Shim Coils	10
Four Jaw Collimator	12
Ion Chamber	12
Ion Chamber Mount	14
Nitrogen Manifold and Temperature Interlock.....	14
Beam Scanning Apparatus	16
Linear Translation Tables	16
Scanning and Alignment Armature	17
Collimation Shield.....	17
Beam Monitor	17
Magnetic Field Mapping Apparatus.....	18
Magnetic field sensor.....	18
V-block.....	18
Magnetometer Sled	20
Alignment laser	20
Polarimetry Apparatus	21

Polarimetry mount.....	21
Collimation Shield.....	21
³ He Spin Filter.....	22
CHAPTER 3: REQUIREMENTS FOR ALIGNMENT	24
Function of the Ion Chamber.....	24
Ion Chamber Requirements.....	26
RFSR Requirements.....	28
Magnetic Field Requirements	30
CHAPTER 4: ALIGNMENT PROCEDURE	31
PRELIMINARY SETUP.....	31
Calibration Technique	32
Alignment Procedure	33
Beam Scanning.....	41
3D Modeling.....	46
Spin Rotator Installation and Alignment	47
Four Jaw Collimator Installation and Alignment	47
Ion Chamber Installation and Alignment	49
CHAPTER 5: CONFIRMATION OF ALIGNMENT.....	56
Commissioning	56
Spin Rotator Efficiency.....	56
Ion Chamber Alignment Check	57
Concluding Remarks.....	58
Works Cited.....	59
Vita	61

LIST OF TABLES

Table 1. Data indicating the magnetic response to current change for individual shim coils.	34
Table 2. Data results from adjustment of left/right shim coil pair. Here, ΔB_x represents the difference between two consecutive measurements following a current adjustment. The shaded row reflects the current that was chosen for the final settings.	36
Table 3. Data results from adjustment of front/back shim coil pair. Here, ΔB_z represents the difference between two consecutive measurements following a current adjustment. The shaded row reflects the current that was chosen for the final settings.	36
Table 4. The magnetic field through the center along the x-axis, transverse to beam direction and gravity.	36
Table 5. Gradients approximated from the field data along the x-axis.....	37
Table 6. The magnetic field through the center along the z-axis.	37
Table 7. Gradients approximated from the field data along the z-axis.....	38

LIST OF FIGURES

Figure 1. The range of the W_{\pm} and Z^0 bosons is too short for direct interaction between nucleons. Instead, the interaction is possible through the decay of π , ρ , and ω . Figure courtesy of Chris Hayes.	4
Figure 2. The strong vertex on the left side of each diagram is associated with the meson coupling constant $h_{\pi 1}$. The exchange of a π^0 is not possible here since neutral spinless mesons do not contribute to parity violation. Figure courtesy of Chris Hayes. ..	6
Figure 3. The ρ^0 and ω^0 are both vector particles. They carry no isospin and no charge so both nucleons at each vertex are the same. Figure courtesy of Chris Hayes.	6
Figure 4. The General configuration of the $n^3\text{He}$ experiment's primary components. The polarimetry apparatus is only used during polarimetry and spin rotator efficiency measurements.	7
Figure 5. The resonant frequency spin rotator (RFSR). Square insets are machined at both ends to 0.040 inches for efficient transmission of neutron beam. (Figure courtesy of Chris Hayes).	11
Figure 6. The internal field of the RFSR. Note the uniformity of the interior field and the fact that the fringing lines are contained within the two cylinders. The exterior field is zero everywhere. Figure courtesy of Chris Hayes.	11
Figure 7. An Autodesk rendering of the exterior of the ion chamber. The cylindrical portion contains the HV and signal planes and the square portions house the pre-amplifier electronics. Figure courtesy of Mark McCrea.	13
Figure 8. The kinematic ion chamber mount.	15
Figure 9. The ion chamber placed upon its mount for fitment and pre-alignment.	15
Figure 10. The beam scanning assembly. The beam monitor and its amplifier are shown in red. The collimation shield is shown in transparent blue.	19
Figure 11. A close-up of the magnetometer (gold) cradled in the sled.	19
Figure 12. The magnetometer and sled placed into the matching groove in V-block.	20
Figure 13. The alignment laser placed on its kinematic mount.	22
Figure 14. The polarimetry apparatus. The ^3He spin filter can be seen resting in the center. The attached Helmholtz coils (AFP coils) are used to flip the spins of the ^3He nuclei in the cell.	23
Figure 15. The HV planes (red) act to drive the desired products of ionization toward the signal planes (blue). Figure courtesy of Chris Crawford.	25
Figure 16. As seen here, the protons range out farther than the much heavier triton. This allows us to distinguish between the two. Figure courtesy of Chris Crawford.	25
Figure 17. Due to the nature of the asymmetry, when the neutron spin is up (orange) the distribution of ionization products is skewed to the top. When the spin is down (blue) the distribution is skewed toward the bottom. The measurement is garnered from the difference in detector output between these two states.	27

Figure 18. Misalignment of the chamber with respect to the spin of the neutrons results in a component of the much larger parity conserving asymmetry along the detector's sensitive axis.....	27
Figure 19. If the RFSR is misaligned by angle δ the spin of the neutron picks up a misalignment of 2δ when it is rotated.	29
Figure 20. A graph of the above data. The slopes of the lines were used as a basis for further adjustments.....	34
Figure 21. An example graph of the above gradient approximations.	37
Figure 22. An example graph of the above gradient approximations.	39
Figure 23. The change in B_x during the transit of the crane.....	40
Figure 24. The change in B_y during the transit of the crane.....	40
Figure 25. The change in B_z during the transit of the crane.....	41
Figure 26. 2D scan of the upstream beam profile. The colors represent the magnitude of the voltage read from the scanner. Figure courtesy of Md. Kabir.....	43
Figure 27. 3D image of the upstream data where the vertical axis (z) is voltage. Figure courtesy of Md. Kabir.	43
Figure 28. . 2D scan of the downstream beam profile. The colors represent the magnitude of the voltage read from the scanner. Figure courtesy of Md. Kabir.....	44
Figure 29. 3D image of the downstream data where the vertical axis (z) is voltage. Figure courtesy of Md. Kabir.	44
Figure 30. As seen above, if the alignment laser is even slightly misaligned it will fail to shine through both alignment holes. Figure courtesy of Chris Hayes.	45
Figure 31. The spin rotator installed at the upstream side of the experiment.	48
Figure 32. The four-jaw collimator installed in front of the spin rotator. The ion chamber mount is visible in the foreground.....	48
Figure 33. The ion chamber being hoisted into place. Note the progress capture pulley (orange). Photo courtesy of Jack Thomison.....	51
Figure 34. The pre-alignment of the ion chamber. The digital protractor which was used to level the chamber can be seen perched on top.....	51
Figure 35. This model typifies the laser alignment of the RFSR, four-jaw collimator, and ion chamber. Only when properly aligned will the laser beam be reflected back precisely to its point of origin.	54

CHAPTER 1:

THEORY AND MOTIVATION

The $n^3\text{He}$ experiment is designed to probe the hadronic weak interaction by measuring the parity violating asymmetry A_p between the spin of incoming neutrons (σ_n) and the momentum of outgoing protons (k_p) following the nuclear break up in the reaction $n+^3\text{He}\rightarrow p+T+765\text{keV}$. There are some difficulties in measuring this quantity due to its predicted small size of approximately 10^{-7} and the fact that the effect is occurring in a regime dominated by the much more intense strong force. As such a brief survey of the forces involved is instructive.

Strong Interaction

In particle physics, the strong interaction is responsible for binding quarks into hadrons such as protons, neutrons, and mesons. It can be described theoretically by quantum chromodynamics which models the interaction as being mediated by gluons, exchanged between quarks, both possessing a property known as color charge. According to the time-energy uncertainty relation, the massless gluon has an infinite range, much like a photon. In addition to infinite range the strength of the strong interaction is relatively static at large distances. In fact, the interaction is so energetic at large distances that when attempting to separate bound quarks that it becomes energetically favorable to create a new pair of quarks which will bind to the originals. This phenomenon is known as color confinement and leads to the fact that free quarks cannot exist, that is, they are always bound within hadrons. Once the quarks are bound

within a hadron the color charge is neutralized, thus the strong interaction is felt only between unbalanced quarks and not between every quark in the universe.

Residual Strong Interaction

From a large distance hadrons appear to be color neutral but at close range there is a minor attraction between separate hadrons thus the effects of the strong force are still felt by hadrons, but to a lesser extent than that between quarks. This residual strong force, otherwise known as the strong nuclear force, is responsible for binding protons and neutrons into a nucleus and is analogous to the van der Waals forces of electromagnetism. At low energy, the nuclear force can be modeled as being mediated by mesons, which are composed of quark-antiquark pairs and can thus transmit the strong force between nucleons. Mesons have mass $\sim 140\text{MeV}$ and as a result have a range of only 10^{-15}m , approximately the size of a nucleon. Beyond this range the force drops off quite rapidly and at distance less than $\sim 0.7\text{fm}$ it becomes repulsive. The strength of the nuclear force is 10^7 times less than that of the strong, due in part to its shorter range and also the fact that the color charge is mostly canceled within the nucleon itself, but is still a great deal larger than the strength of the weak interaction.

Weak Interaction

The weak interaction acts on particles possessing the property of flavor charge i.e. quarks and leptons. It is mediated by the intermediate vector bosons W^\pm and Z^0 , with masses of 80GeV and 91GeV respectively, and thus has an extremely short range of only 10^{-18}m . Relative to the strong force, the strength of the weak force is 10^{-6} times smaller.

Parity Violation

A parity inversion is one that reverses the sign of the spatial coordinates of a system. If an observable of the system maintains its sign under a parity transformation it is said to conserve parity, those that change sign are said to violate parity. Of the four fundamental forces, gravitational, electromagnetic, strong, and weak, only the weak force is known to be parity violating. As a result, parity symmetry violation can be used as a hallmark to identify weak interactions in strong dominated regimes.

Hadronic Weak Force

As seen from the above sections, both quarks and leptons experience the weak interaction. The leptonic weak interaction is well understood, due in part to the fact that it is possible to observe unbound leptons, but the weak interaction among quarks is far more difficult to quantify. Since a quark is always bound within a hadron any attempt to observe the weak quark-quark interactions must be done in a hadronic context, that is to say, in the presence of the much more powerful strong force. Furthermore, the repulsive nature of the nuclear force at close ranges effectively limits the distance between nucleons to values far greater than the range of the weak force and suppresses nucleon-nucleon contact. However, since the strong force conserves parity, any parity violating effects that are observed can be attributed wholly to the presence of weak interactions.

The exact details of the apparent correlation between weak and strong effects are not well understood but it is clear that an appropriate treatment requires a theory that simultaneously considers weak and strong effects. The long term success of the

meson exchange model in describing the nuclear force represents a plausible mechanism for the mediation of nuclear forces as well as weak, although there has been some difficulty in deriving this from the standard model. The classic treatment was presented in a paper published in 1980 by Desplanaques, Donoghue, and Holstein (DDH) [1]. In their interpretation, the strong interaction between hadrons is mediated by light virtual mesons which then decay weakly before coupling to the second vertex (Figure 1).

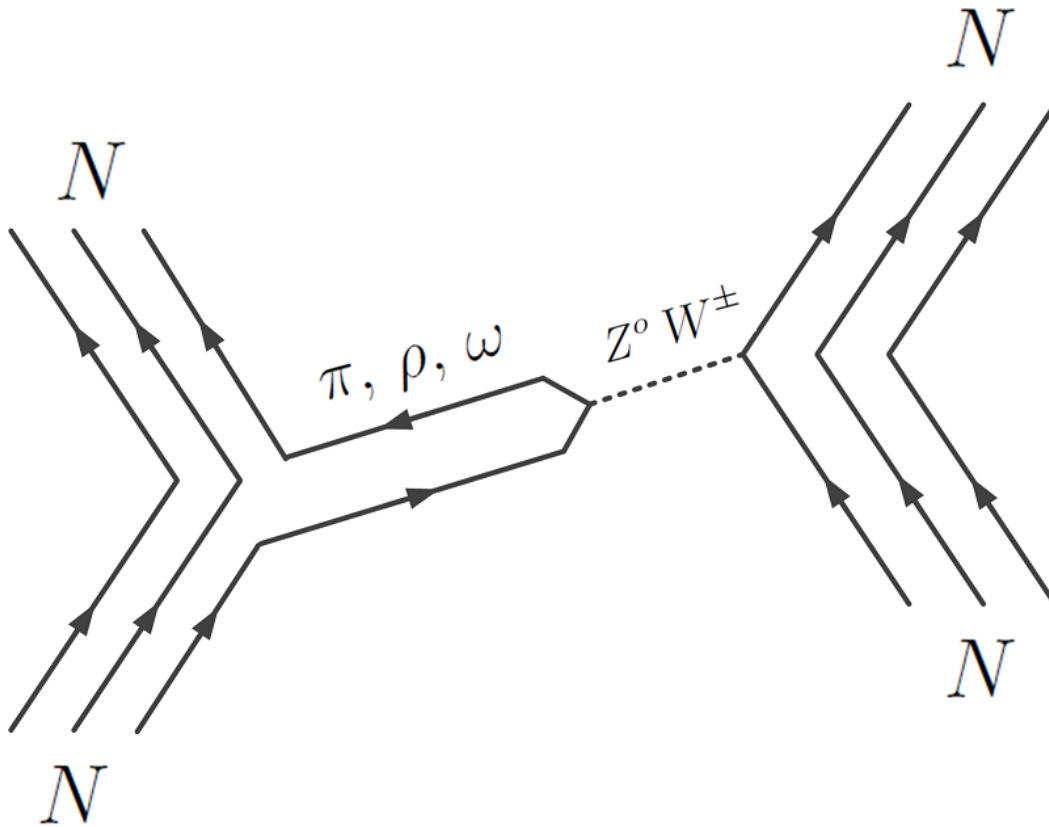


Figure 1. The range of the W^\pm and Z^0 bosons is too short for direct interaction between nucleons. Instead, the interaction is possible through the decay of π, ρ , and ω . Figure courtesy of Chris Hayes.

The authors relate the parity violating observables to weak meson-nucleon coupling constants. The most general form of observables in this model are constructed of six unknown coupling constants which must be experimentally determined, although reasonable ranges of the values are predicted. The general expression for an parity violating observable may be written as

$$A = a_{\pi}^1 \cdot h_{\pi}^1 + a_{\rho}^0 \cdot h_{\rho}^0 + a_{\rho}^1 \cdot h_{\rho}^1 + a_{\rho}^2 \cdot h_{\rho}^2 + a_{\omega}^0 \cdot h_{\omega}^0 + a_{\omega}^1 \cdot h_{\omega}^1$$

Where the “a” terms are determined by the particular experiment and the “h” terms are the weak coupling constants to be measured. The subscripts indicate the type of light virtual meson and the superscripts are the weak isospins. It is the goal of the $n^3\text{He}$ experiment to verify the nucleon-nucleon meson exchange model of DDH by measuring some of these coupling constants.

The observable for the $n^3\text{He}$ experiment is A_p , the parity violating asymmetry between the spin of incoming neutrons (σ_n) and the momentum of outgoing protons (k_p) following the nuclear break up in the reaction $n+^3\text{He} \rightarrow p+T+765\text{keV}$. While all six coupling constants from above contribute, only three are significant, which leads to the approximation

$$A_p = -0.18 \cdot h_{\pi}^1 - 0.14 \cdot h_{\rho}^0 - 0.13 \cdot h_{\omega}^0$$

The h_{π}^1 coupling constant was measured by the NPDGamma collaboration so our aim is the measurement of the zero isospin coupling constants h_{ρ}^0 and h_{ω}^0 . Feynman diagrams associated with relevant constants are shown in Figure 2 and Figure 3 [2]. Due to the overwhelming dominance of the strong interaction it is paramount that the

systematic uncertainties inherent in the experimental apparatus be carefully controlled to avoid false asymmetries in the data. It is chiefly with these uncertainties that the following alignment procedure is concerned.

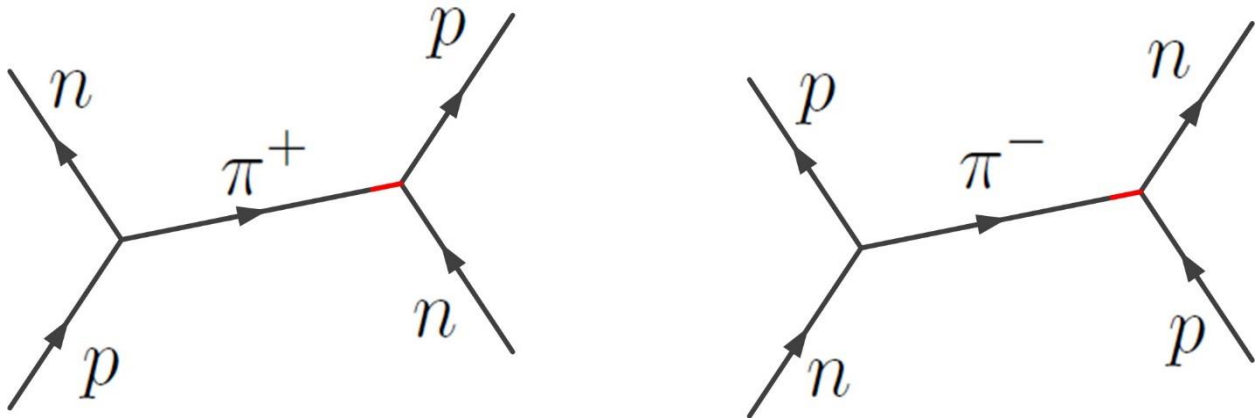


Figure 2. The strong vertex on the left side of each diagram is associated with the meson coupling constant h_{π}^1 . The exchange of a π^0 is not possible here since neutral spinless mesons do not contribute to parity violation. Figure courtesy of Chris Hayes.

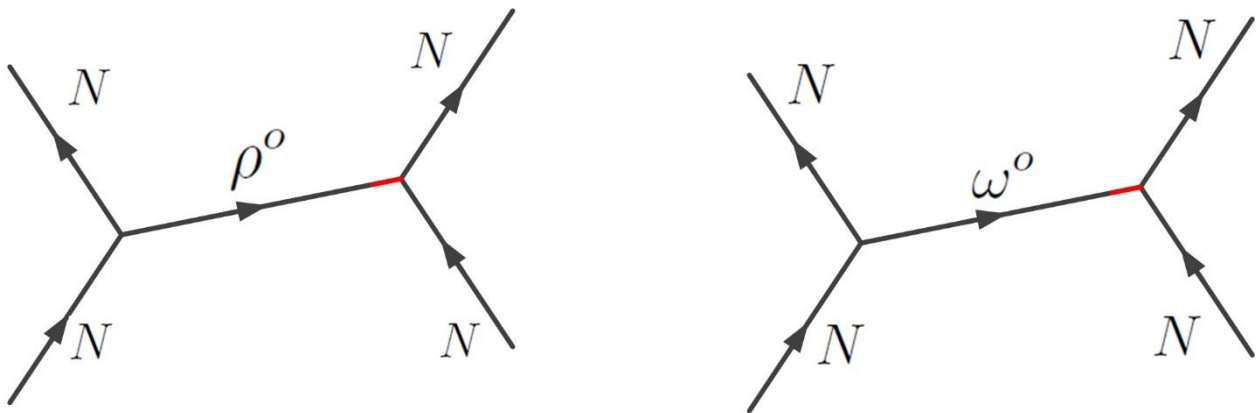


Figure 3. The ρ^0 and ω^0 are both vector particles. They carry no isospin and no charge so both nucleons at each vertex are the same. Figure courtesy of Chris Hayes.

CHAPTER 2: EXPERIMENTAL APPARATUS

Experimental Overview

Thermal neutrons from the SNS are passed through a super mirror polarizer which absorbs one spin state and passes the other. Essentially all neutrons (96%) exiting the downstream end are polarized spin up. The neutrons are then allowed to pass through a resonant frequency spin rotator which alternately inverts the spin state (on) or allows them to pass through unchanged (off). The neutron beam then passes through a collimator at which point it enters the ^3He ion chamber. When a ^3He nucleus absorbs a neutron it decays producing a triton, a proton, and 0.765 keV kinetic energy shared between them. The energetic charged particles ionize the gas and the products of ionization are detected by an array of signal wires. The general configuration of the primary components is shown in Figure 4.

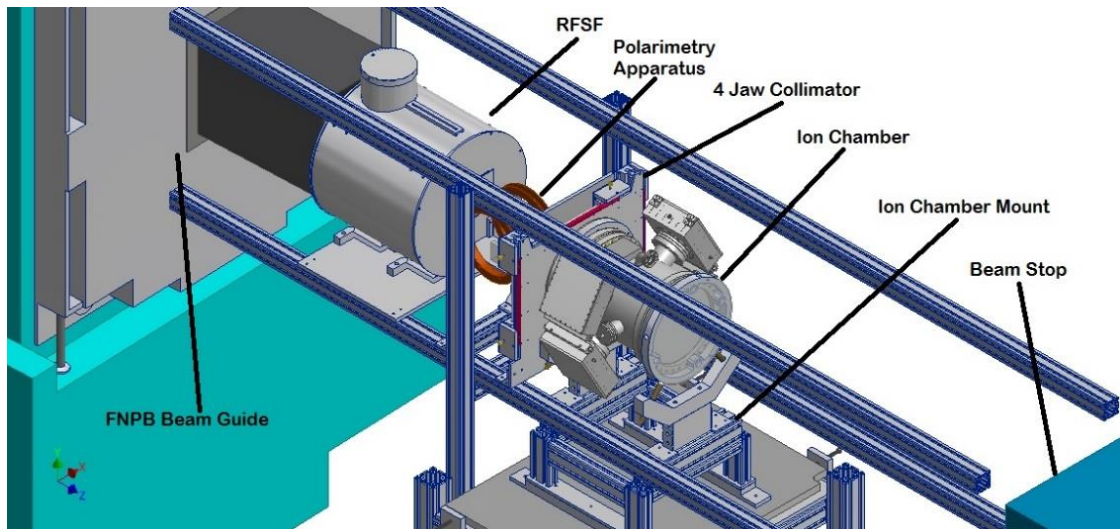


Figure 4. The General configuration of the $n^3\text{He}$ experiment's primary components. The polarimetry apparatus is only used during polarimetry and spin rotator efficiency measurements.

Neutron Production

Neutron production at the SNS begins with a source of negative hydrogen ions. The negative ions are injected, in pulses, into an accelerator which accelerates them to (2.5MeV) and then the passed to a linear accelerator, or LINAC, which further accelerates them to approximately 1GeV. The ions are then passed through a series of thin metal foils to strip off the electrons producing a beam of H⁺ ions (protons). These protons are shunted into an accumulator ring where they are “spooled” around approximately 1200 times, bunching them together. When the entire LINAC pulse has been stored in the accumulator ring the protons are released and projected toward the target 60 times a second. The target consists of a large vessel or “thimble” containing liquid mercury. When a high energy proton impacts a mercury nucleus, dozens of neutrons are ejected. These neutrons are moderated to lower energy by being passed through vessels of LH2 and are then guided to the experiment hall for research [3].

Frame Definition Choppers

After leaving the moderator, the beam contains neutrons with a very broad velocity distribution and in the region between the moderator and the target it is possible for the faster neutrons from one pulse to overtake the slower neutrons from the pulse ahead thus obscuring and mixing separate pulses. As a well-defined pulse width is necessary for efficient spin flip ratio this is undesirable. To mitigate this effect two frame definition choppers are utilized to select only a portion of the beam by stopping both the fastest and slowest neutrons of each pulse. The choppers themselves consist of large aluminum disks, rotating about an axis parallel to the beam, onto which a paint containing ¹⁰B has been applied excluding a sector with opening angle θ which has

been cut from the disk to allow passage of neutrons [4]. Neutrons impacting the painted surface are absorbed and those passing through the cut out are transmitted. The choppers are rotated at the pulse rate of the beam (60Hz). By selection of appropriate opening angles of the removed sectors, wrap-around neutrons can be eliminated and a well-defined pulse width maintained.

Supermirror Polarizer

The supermirror polarizer is composed of ultra-thin alternating lamina of nickel and titanium laid on a thin (~0.3mm) substrate of borated glass. These lamina are situated in a uniform magnetic field, on the order of 300 Gauss, which magnetizes the nickel layers to saturation. As neutrons enter the lamina, the neutron magnetic moment interacts with the effective field in such a way that neutrons of one spin state reflect toward the target chamber, and neutrons of the other spin state are transmitted and subsequently absorbed by the substrate. The reflected neutrons emerge with a greater than 96% net polarization [4].

Resonant Frequency Spin Rotator

The resonant frequency spin rotator is a device which uses spin magnetic resonance to periodically invert the spin of incoming neutrons. A large aluminum cylinder houses a double cosine-theta coil which is characterized by its extremely uniform interior magnetic field [2], for efficient spin rotation, and zero exterior field, to maintain the uniformity of the holding field and to avoid spurious effects. The interior of the sealed cylinder is filled with ^4He gas, which has an extremely low cross section for capture of thermal neutrons and allows neutrons to pass through the interior of the

cylinder without scattering. The spin rotator and a diagram of its magnetic field are shown in Figure 5 and Figure 6, respectively.

Magnetic Holding Field

The holding field is generated by a set of four large rectangular wire coils, approximately 1.5 m x 3 m, encompass the entire experimental apparatus, oriented in horizontal planes. The middle pair, spaced 0.5 m apart, have 50 turns of wire with a total current 21A apiece and are largely responsible for both the magnitude and direction of the main holding field. The outer pair, spaced 2 m apart, have 20 turns of wire and also have a current of 21A apiece and serve to improve the uniformity of the holding field by minimizing fringing effects. Together these coils generate an approximately 9 gauss magnetic field in the vertical direction. The purpose of this field is to maintain the polarization of the neutron beam after it exits the super mirror polarizer and to maintain the polarization of the ^3He cell used for polarimetry measurements.

Magnetic Shim Coils

The shims are smaller coils (in terms of current capacity) placed in vertical pairs both parallel and transverse to the beam direction. The parallel pair measure 2 m x 3 m and have approximately 50 turns of wire. The transverse pair measure 1.5 m x 2 m and have approximately 60 turns of wire. Both pairs have total currents on the order of hundreds of milliamps. By simultaneously adjusting the current flowing through matched pairs, small deviations in the direction of the main field may corrected. Current adjustments of a single coil allow for control of the gradients.

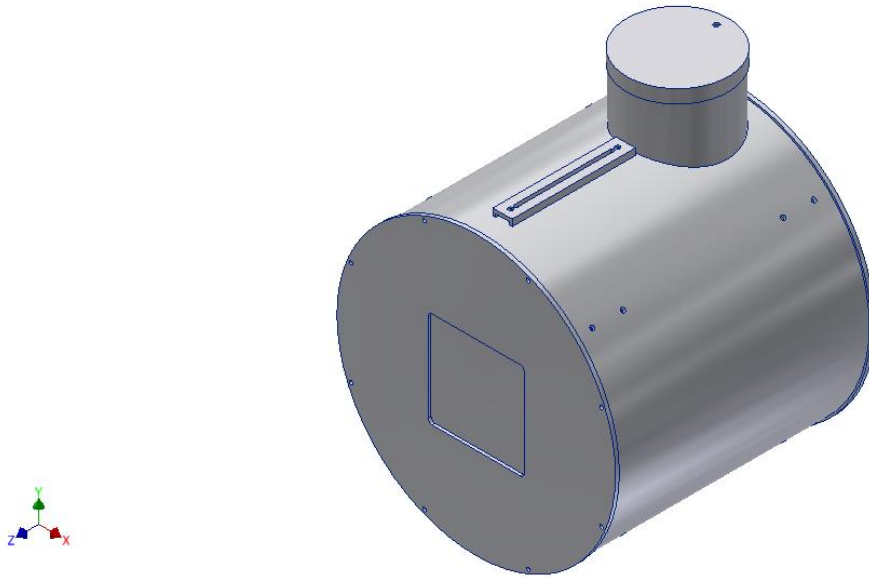


Figure 5. The resonant frequency spin rotator (RFSR). Square insets are machined at both ends to 0.040 inches for efficient transmission of neutron beam. (Figure courtesy of Chris Hayes).

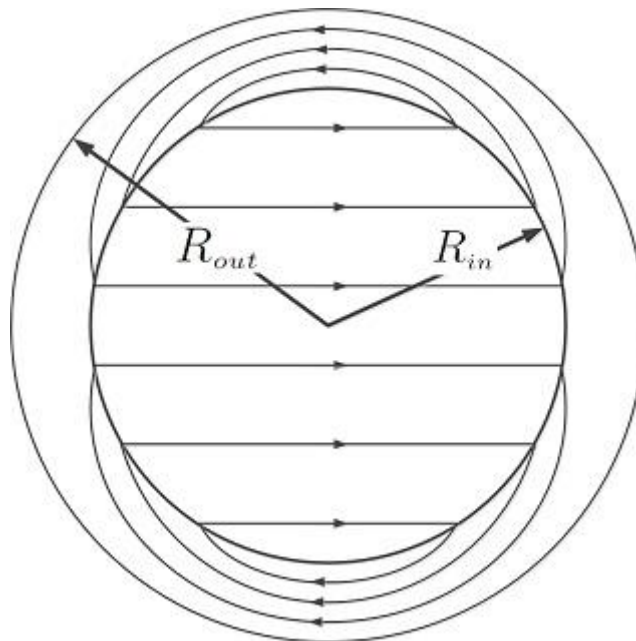


Figure 6. The internal field of the RFSR. Note the uniformity of the interior field and the fact that the fringing lines are contained within the two cylinders. The exterior field is zero everywhere. Figure courtesy of Chris Hayes.

Four Jaw Collimator

The collimator is a simple device consisting of four adjustable panels, a pair in the vertical direction and a pair in the horizontal direction, which is used to collimate the neutron beam prior to entering the target chamber. The panels are clad in a layer of cadmium and a layer of lithium. The lithium layer absorbs 99% of neutrons incident upon it and the cadmium layer serves to absorb the remainder. The collimation of the neutron beam is necessary to reject the outer edge of the beam, which is diverging more rapidly, and could lead to false asymmetries.

Ion Chamber

This device serves as both the target and detector for the $n^3\text{He}$ experiment. It is a multi-wire ionization chamber with 33 parallel planes of wires, 16 signal planes and 17 high voltage planes. The Ion Chamber is filled to 0.5 atmospheres with ^3He and is placed upon a specially built kinematic mount at the center of the neutron beam. When an incident neutron is captured by a ^3He nucleus it spontaneously decays into a proton and a triton. As the proton and triton lose energy in the gas they ionize it. The high voltage planes are held at negative bias with respect to the grounded signal planes. As a result the positively charged ions are drawn towards the high voltage planes and the negatively charged ions are driven toward the signal planes where they are collected and form currents in the signal wires. The signal wires are routed to four pre-amplifiers located in temperature controlled enclosures located radially on the exterior of the ion chamber housing. The ion chamber is shown in Figure 7.

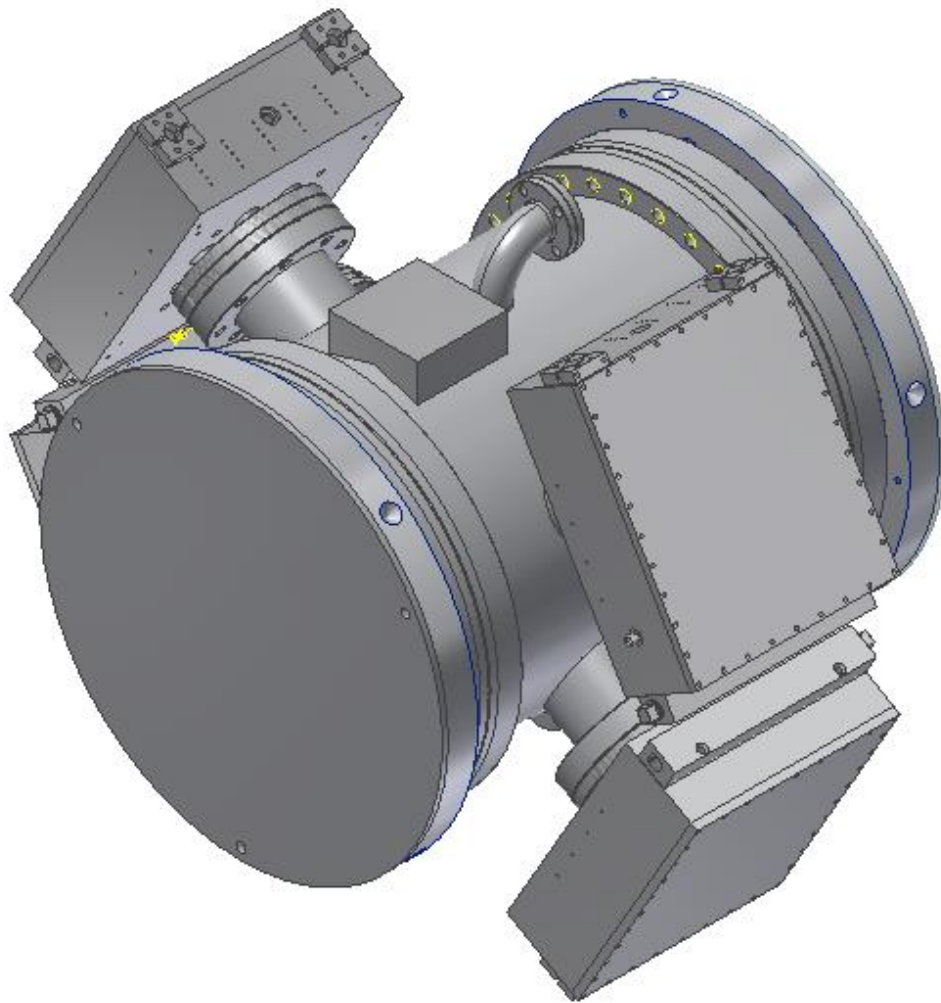


Figure 7. An Autodesk rendering of the exterior of the ion chamber. The cylindrical portion contains the HV and signal planes and the square portions house the pre-amplifier electronics. Figure courtesy of Mark McCrea.

Ion Chamber Mount

As the commissioning phase requires multiple insertions and extractions of the chamber and the experiment itself requires several 90 degree rotations to measure a separate parity conserving asymmetry, a mounting solution was required that would accommodate these moves while alleviating the need perform a separate alignment each time. To that end a robust kinematic mount was designed and constructed specifically to carry the ion chamber. It consists of two cradles each of which is fitted with a pair of 1 inch threaded rods into the ends of which have been machined conical depressions. The conical depressions are designed to carry highly spherical ceramic balls, which act as the contact points between the mount and chamber. On the ends of the ion chamber are circular rings into which a series of matching conical depression have been machined. The depressions on the rings are spaced such that one ceramic sphere always lies within a cone while the other three rest on the face of the ring. By adjusting various combinations of the threaded rods the yaw, pitch, and roll of the ion chamber can be adjusted quite accurately. The mount is shown in figures 8 and 9.

Nitrogen Manifold and Temperature Interlock

The electronics of the pre-amps generate a large amount of heat which, if left unchecked, could result in their failure. The fact that they are each enclosed in a protective housing only further exacerbates the problem. To address this issue a cooling system was installed which passes a constant stream of room temperature nitrogen through the pre-amp enclosures. Nitrogen is fed from an external tank into a manifold which divides the stream to the four enclosures as needed. Each of the individual feed lines is equipped with an analog flow meter and the total flow can be read remotely from

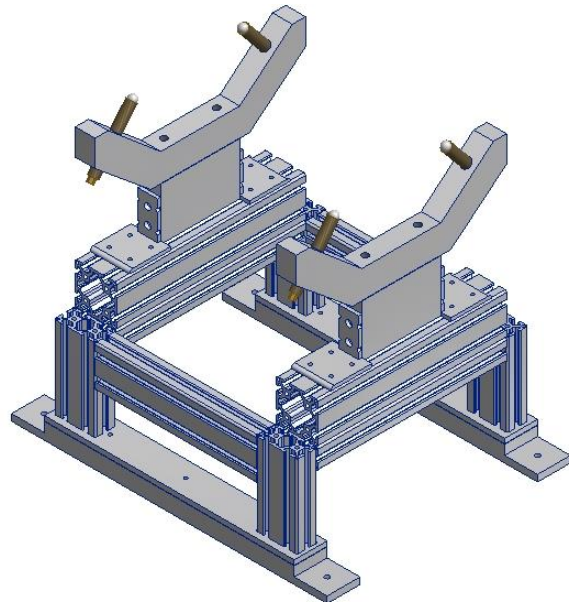


Figure 8. The kinematic ion chamber mount.

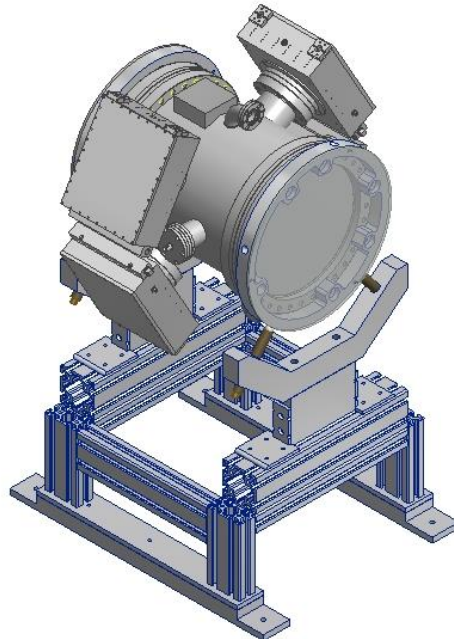


Figure 9. The ion chamber placed upon its mount for fitment and pre-alignment.

a digital flow meter. To further guard the system from damage an interlock device was utilized which severs the power connection to the pre-amps in the event that the temperature becomes too high or the nitrogen flow becomes too low.

Beam Scanning Apparatus

In order to maximize counting statistics and eliminate false asymmetries it is required that all of the major experimental components be precisely aligned to the neutron beam axis. To do this it required that the centroid of the beam be located at two locations. A line between these two points is then sufficient to uniquely define the direction of the beam. The beam centroid was determined by mapping the beam intensity at approximately 1cm intervals using a beam scanning apparatus designed specifically for this purpose. Its basic components are as follows.

Linear Translation Tables

Four Velmex Bi-Slide linear translation tables were utilized to carry the alignment armature and beam monitor. Each table is equipped with a computer controlled high precision stepper motor capable of steps of less than 10^{-5} m. The tables were coupled together in pairs such that one table, which translates horizontally, carries upon it the other table, which translates vertically. The coupled pairs were installed such that the translation axes of both were perpendicular to the beam direction. This configuration allows for raster scanning by iteration over the full range step sizes of one axis for each step size of the other axis.

Scanning and Alignment Armature

There are two specially designed aluminum armatures, one for each pair of tables, providing a secure and stable mounting surface for the beam monitor and preamplifier. Each armature is outfitted with a laser alignment port. These ports are accurately offset below and to one side of the beam monitor and can be aligned to provide a clear line of sight from one end of the experiment to the other.

Collimation Shield

The collimation shield is a lithium clad aluminum plate which attaches to the beam side of the scanning and alignment armature. A 1 cm square hole, which coincides with the center of the beam monitor, is cut through the plate. The purpose of this device is twofold. It provides a known cross section of small enough size to ensure an acceptable resolution of data and it helps prevent scattering of neutrons off of the air in the experiment hall as the lithium cladding absorbs 99% of the neutrons incident upon it.

Beam Monitor

The beam monitor is a multi-wire ionization chamber which is used to measure the intensity of the neutron beam. It operates upon the same principles as the ion chamber, albeit in a somewhat simplified manner. A frame containing equally spaced, grounded, parallel signal wires is sandwiched between two other planes containing equally spaced high voltage wires. The frame assembly is sealed inside an enclosure and filled with a small amount of ^3He gas. When a neutron enters the monitor it is captured by a ^3He nucleus which decays into a proton and a triton. As the proton and triton travel through the gas they cause it to ionize. The high voltage planes are held at a negative bias with respect to the grounded signal planes and as a consequence, the

positively charged ions will travel toward the high voltage planes and the negatively charged electron will be driven toward the signal plane which will register a current that is proportional to the intensity. This current is subsequently fed to a preamp and the data recorded by a computer. When coupled with the aforementioned translation tables and alignment armature, the beam monitor may be utilized to locate the centroid of the neutron beam by averaging over the measured intensity profile. The beam scanning apparatus is shown in Figure 10.

Magnetic Field Mapping Apparatus

Since the asymmetry that is to be measured is associated with the main holding field, in that it defines the quantization axis for the spin of the neutrons, detailed knowledge of the field's magnitude, direction, and gradients is required. In order to map the field an apparatus was required that was robust enough to remain aligned while in use but that would also facilitate the movement of the magnetometer to different locations. The components of this apparatus are discussed below and models are shown in Figure 11 and Figure 12.

Magnetic field sensor

A Bartington MAG-03MS three-axis magnetic field sensor which produces a voltage output proportional to magnetic field strength was used to map the field. It reports the data to a computer via a long serial cable and can measure fields up to 10G.

V-block

The V-block consists of a long (72") aluminum block into which a 90 degree channel has been machined. Its purpose is to provide a solid base for the

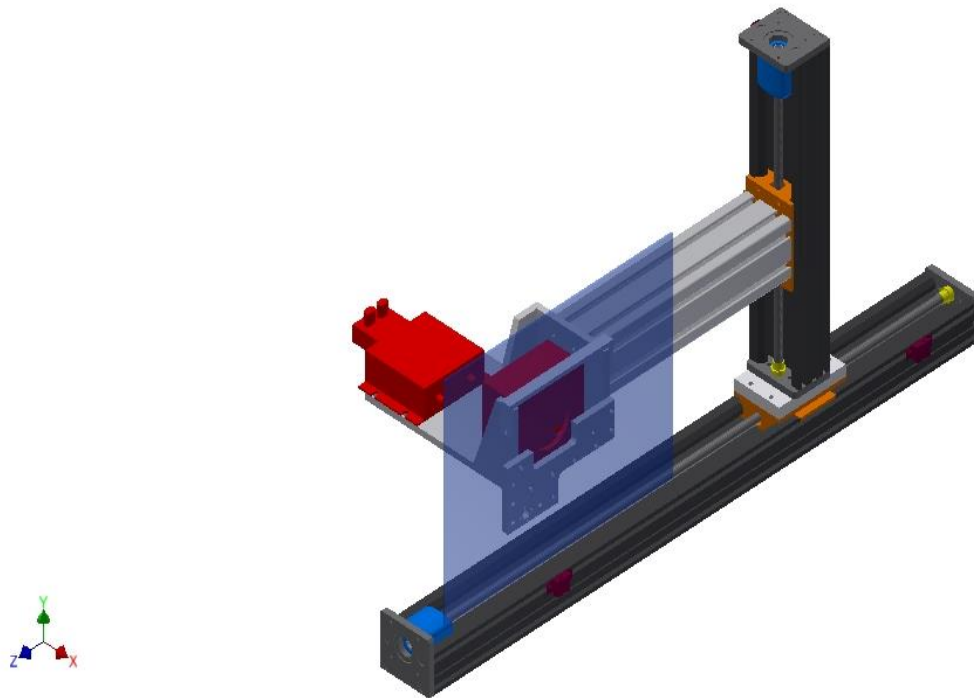


Figure 10. The beam scanning assembly. The beam monitor and its amplifier are shown in red. The collimation shield is shown in transparent blue.

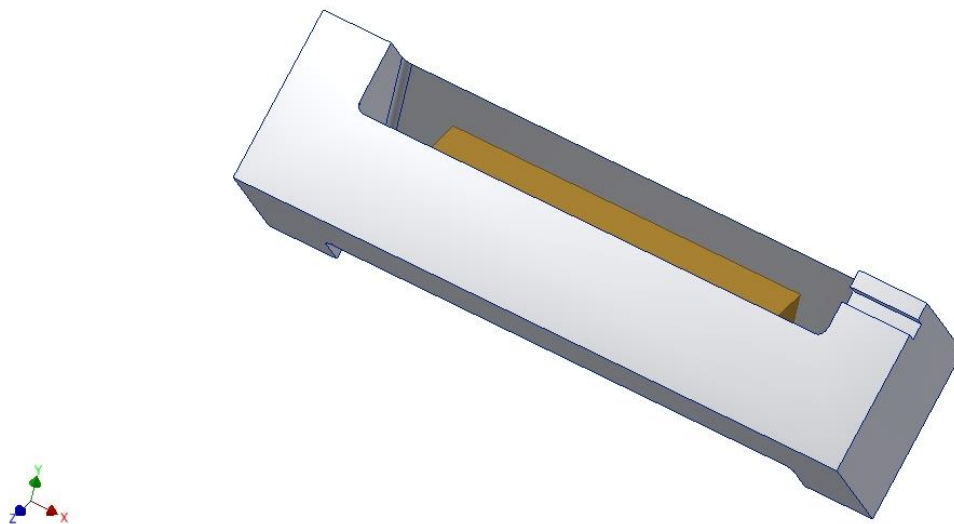


Figure 11. A close-up of the magnetometer (gold) cradled in the sled.



Figure 12. The magnetometer and sled placed into the matching groove in V-block.

magnetometer sled and ensure that consecutive measurements of the magnetic field are taken along the same axis. It may be mounted either parallel or perpendicular to the beam and allows the sled to be placed at any desired location inside of the main holding field. Prior to use the V-block is precisely leveled with respect to gravity.

Magnetometer Sled

The sled is a machined aluminum block to which the magnetometer is attached. When coupled with the V-block it ensures that the probe's coordinate system is aligned with the experimental coordinate system. The sled is constrained within the V-block such that it may only translate along its longest axis.

Alignment laser

This laser is located in the beam stop is an alignment laser on a kinematic mount. Once the centroid has been located the laser is aligned to shine through the

alignment holes on the scanner armatures after which point it can be used to align the spin flipper and most importantly the target chamber for the most efficient use of the beam profile. The alignment laser is shown in Figure 13.

Polarimetry Apparatus

In order to ensure the continued integrity of the data taken during the experiment it is essential to monitor the polarization of the neutron beam. As such, polarization measurements are to be taken at periodic intervals throughout the duration of the experiment. The apparatus that is to be used to collect this data is a piece of legacy equipment from the NPDGamma experiment that has been modified and adapted to fit the current experiment. The primary components of the apparatus are discussed below and it is shown in Figure 14.

Polarimetry mount

The polarimetry mount is an aluminum frame which provides a mounting surface for the ^3He spin filter cell, pre-amp, and AFP coils. It is equipped with the ability to adjust its position in the horizontal direction, transverse to the beam, as well as a set of three upright supports which can be used to select its height.

Collimation Shield

The collimation shield is a lithium clad aluminum plate with an approximately 5 cm aperture through which neutrons may pass. This aperture is slightly smaller than the 7.5 cm diameter of the spin filter. This shield prevents the unwanted scattering of neutrons while still allowing a small portion of the beam to be utilized for polarimetry.

^3He Spin Filter

The spin filter consists of a small glass cylinder containing ^3He which has been polarized via the process of spin exchange optical pumping, the polarization of which can be maintained for several days by inserting the cell in a magnetic holding field [4]. The ability to invert the polarization of the ^3He within the cell coupled with the strong spin dependence of neutron transmission though it make it well suited to analyzing the polarization of the beam and measuring the spin rotator efficiency .

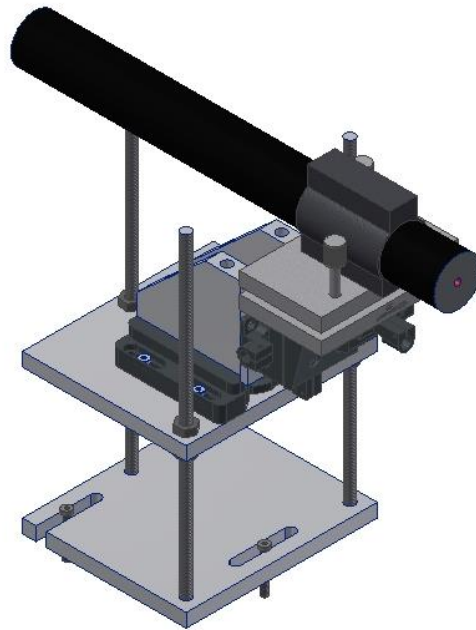


Figure 13. The alignment laser placed on its kinematic mount.

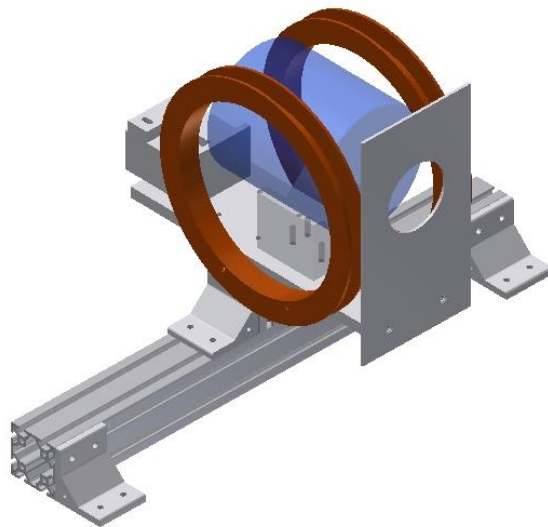


Figure 14. The polarimetry apparatus. The ^3He spin filter can be seen resting in the center. The attached Hemholtz coils (AFP coils) are used to flip the spins of the ^3He nuclei in the cell.

CHAPTER 3: REQUIREMENTS FOR ALIGNMENT

Function of the Ion Chamber

As the alignment requirements for this experiment are derived largely from the geometry of the ion chamber a deeper understanding of its basic theory of operation and arrangement of its internal components is instructive. At the center of the chamber are a series of wires oriented along the x-axis and arranged such that they lie in planes which are perpendicular to the beam direction. Each plane contains either sensor wires or high voltage wires with the two types alternating along the beam axis. The sensor wires collect the electrons that result from the ionization of the ^3He but are insufficient on their own to collect the majority as it is possible for a given electron to miss the wire entirely. To ensure that a sufficient amount of electrons are collected each sensor plane is sandwiched between two high voltage planes, held at large negative bias with respect to the signal plane. These high voltage planes act to drive the negative ions toward the signal planes where they are much more likely to be picked up. The repeating of this structure adds depth to the chamber and provides sufficient volume of gas to ensure all neutrons are absorbed and most of the products of ionization are collected. A representation of this system is shown in Figure 15. Though both the proton and triton ionize the gas, the proton carries $\frac{3}{4}$ of the energy and leaves a trail approximately five times longer than the triton making it easy to distinguish between the two (Figure 16). Since protons with a larger angle with respect to the neutron spin have a greater Δz , the

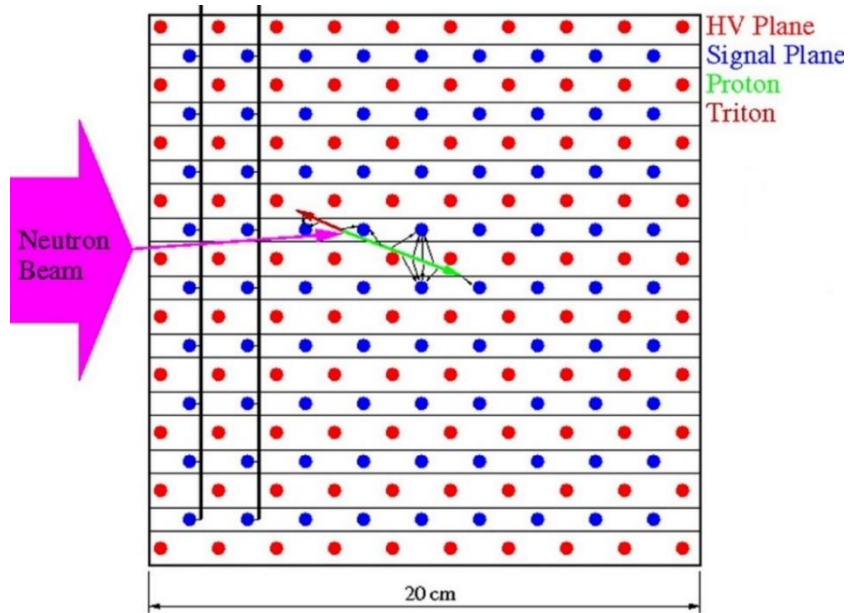


Figure 15. The HV planes (red) act to drive the desired products of ionization toward the signal planes (blue). Figure courtesy of Chris Crawford.

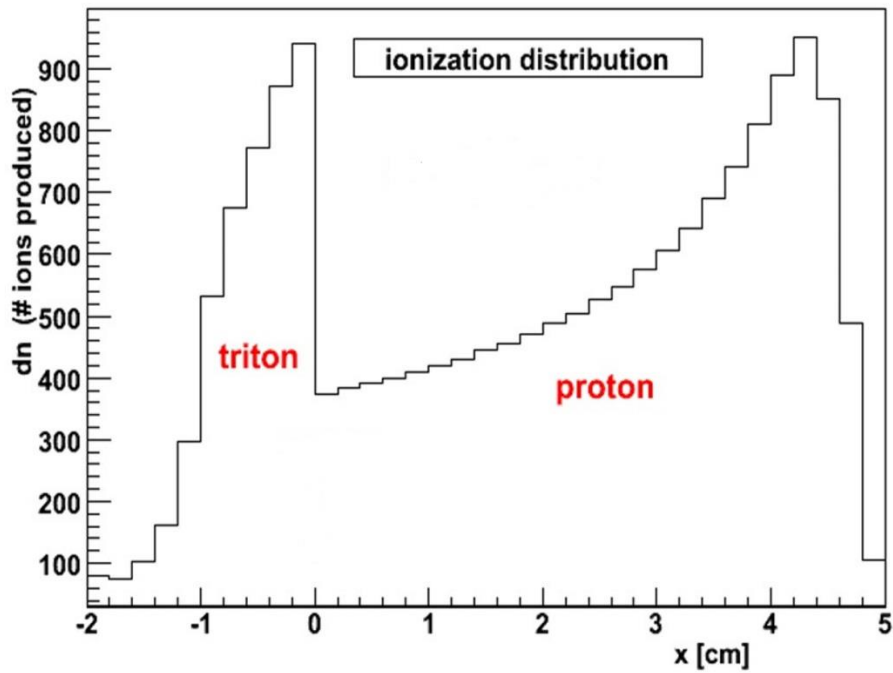


Figure 16. As seen here, the protons range out farther than the much heavier triton. This allows us to distinguish between the two. Figure courtesy of Chris Crawford.

scattering angles can be determined by the depth to which the protons penetrate. The actual measurement of the asymmetry is obtained from the difference in detector output between the two spin states (Figure 17). It is important to note that, since the individual wires run along the horizontal (x) axis the detector is only sensitive in the up-down direction. This is the sensitivity axis of the detector and must be parallel to neutron spin. This constraint leads to the first alignment requirement.

Ion Chamber Requirements

In addition to the desired up-down parity violating asymmetry, there is a parity conserving left-right asymmetry which is on the order of 10^{-6} . As aforementioned, the sensitive axis must be parallel to the neutron spin. This is necessary to avoid mixing of the two effects which could lead to the measurement of a false asymmetry. As seen in Figure 18, a misalignment of the chamber and neutron spin results in a component of the parity conserving asymmetry along the detector's axis of sensitivity. Since a measurement of $\sim 10^{-8}$ is desired this component must be $\sim 10^{-9}$. As seen in Figure 18, the magnitude of this component is given by

$$P.C._{detector} = 10^{-6} \sin(\delta)$$

where delta is the angle between the axis of sensitivity and the spin of the neutrons.

Imposing the desired magnitude we may write

$$10^{-6} \sin(\delta) \sim 10^{-9}$$

Since δ will be small we may use the small angle approximation and write

$$\delta 10^{-6} \sim 10^{-9}$$

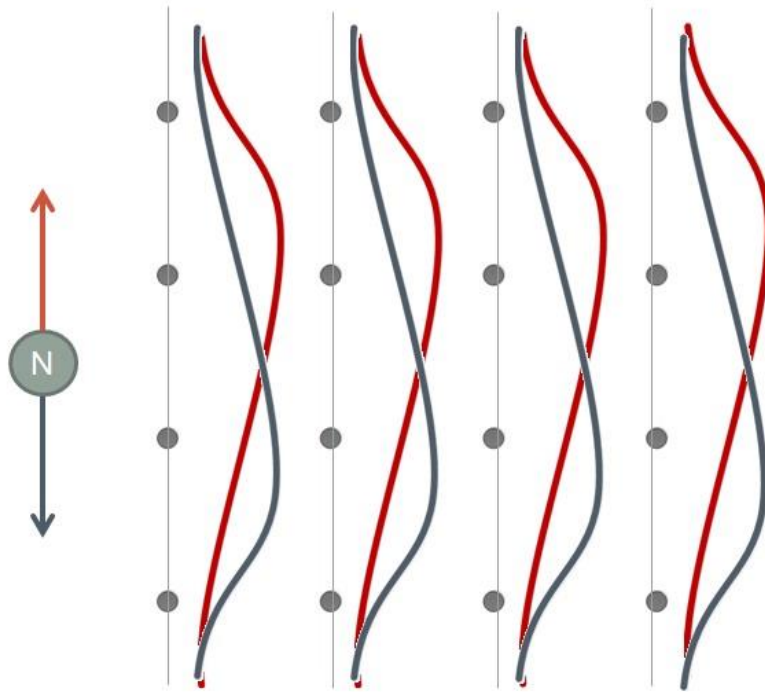


Figure 17. Due to the nature of the asymmetry, when the neutron spin is up (orange) the distribution of ionization products is skewed to the top. When the spin is down (blue) the distribution is skewed toward the bottom. The measurement is garnered from the difference in detector output between these two states.

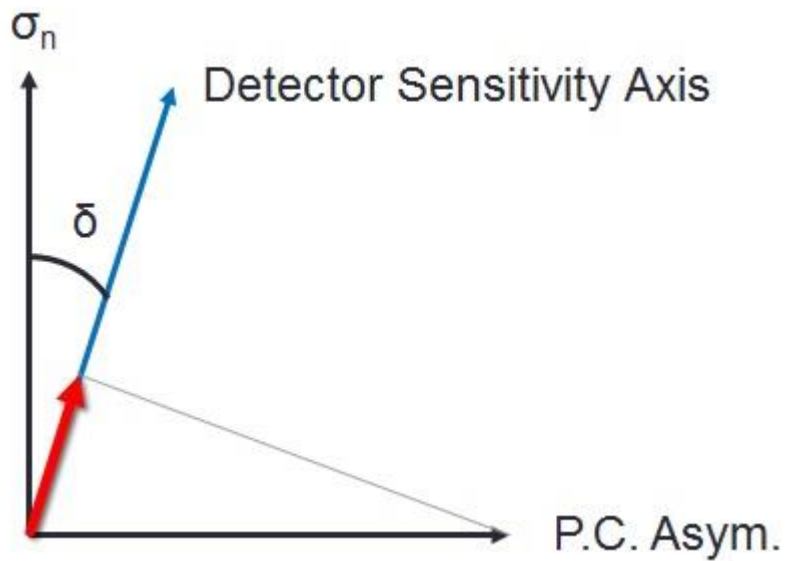


Figure 18. Misalignment of the chamber with respect to the spin of the neutrons results in a component of the much larger parity conserving asymmetry along the detector's sensitive axis.

Which yields the alignment requirement

$$\delta \sim 10^{-3}$$

So the misalignment angle δ must be on the order of 10^{-3} radians to suppress mixing the parity conserving asymmetry to a level where it does not interfere with the measurement of the parity violating asymmetry. The ion chamber is relatively insensitive to pitch and yaw misalignments as these only slightly increase or decrease the distance that a proton travel before being sensed.

RFSR Requirements

It is the function of the spin rotator to rotate the direction of the neutron spin by exactly π radians when switched on. As can be seen in Figure 19, if the field generated by the RFSR is not perpendicular to the spin of the incoming neutrons then when it is switched on they will precess about an axis that is not perpendicular to the original spin and will be left pointing in an undesired direction, specifically it will have picked up an error of 2δ . Since there are only two possibilities for the spin states in the z-direction, up or down, this has the effect of decreasing the probability of finding the rotated particles in the desired state. The probability of finding the improperly rotated neutrons in the desired state, that is spin down, may be approximated by examining the projection of the new spin vector onto the $-z$ axis, a first order approximation is therefore given by expanding the cosine and neglecting higher order terms which gives us

$$P = 1 - 2\delta^2$$

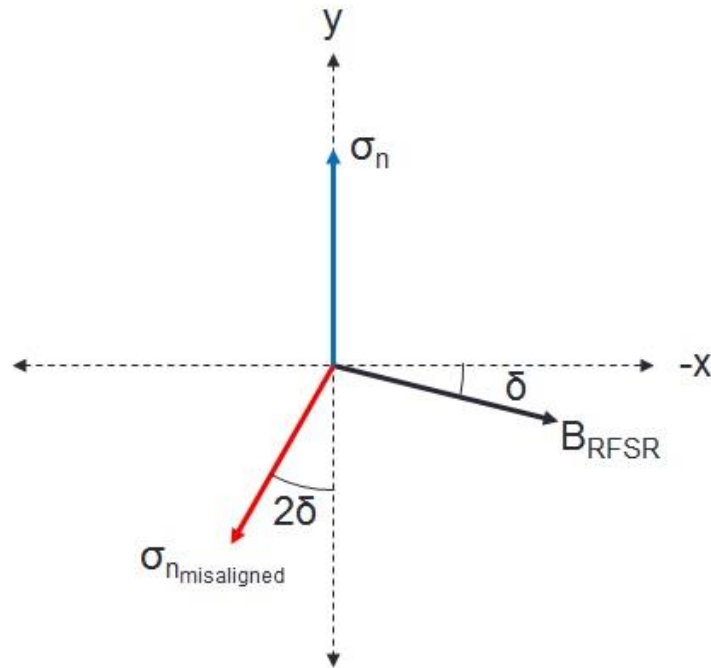


Figure 19. If the RFSR is misaligned by angle δ the spin of the neutron picks up a misalignment of 2δ when it is rotated.

But since δ will be very small, on the order of a few milliradians, and is squared in both equations this factor has minimal impact across the desired range. It is desired to maximize this equation but a physical limitation exists in the digital protractor used to level the RFSR, which has a sensitivity of 0.01 degrees, or about 0.00028 radians. Plugging in this requirements yields a probability of nearly 100% and it is easily seen that misalignments of as great as 4 degrees (nearly 80 milliradians) yield probabilities of greater than 99%. In practice an alignment error of no more than 10^{-3} radians is both readily achievable and more than sufficient for our purposes. The RFSR is insensitive to pitch and yaw misalignments as these leave the perturbing field still perpendicular to the spin direction.

Magnetic Field Requirements

As the main holding field defines the quantization axis for the spins it must be precisely aligned. It is convenient to align the field to local gravity since this allows the use of conventional leveling tools to align the primary components. The precision of the magnetometer readings is bounded by the precision of the digital protractor. Further errors are taken care of by the calibration process. Since the ion chamber is aligned with respect to gravity and must have its sensitive axis parallel to the field the same level of precision is required i.e. 10^{-3} radians. The magnitude of the main holding field must be on the order of 9 gauss, this being sufficient to both strongly define and maintain the quantization axis of the neutron spins and required by the design of the RFSR. In addition, it is required that the field be very uniform in the region containing the spin flipper and the target chamber, that is to say that the gradients along the beam path be very small, on the order of 1mG/cm.

CHAPTER 4:

ALIGNMENT PROCEDURE

PRELIMINARY SETUP

At the beginning of the installation phase the support structure carrying the main holding coils and the heavy duty aluminum table that now holds the ion chamber were already installed in the experiment hall, being legacy equipment from the NPDGamma experiment which previously inhabited the space. In order to install the experiment several additions and modifications were made and steps were taken to reinforce the structure. The shielding was removed from the roof of the experiment hall and a longitudinal support structure was lowered into place via crane. This support structure, which will carry all of the experiments primary components, was centered about the presumed beam path and fastened to the preexisting coil frame. The roof shielding was then replaced and shims were placed between the vertical members of the main coil frame and the ceiling adding rigidity to the structure and strengthening it against lateral movement.

To avoid the longitudinal supports bowing from the weight of the experimental components, vertical support were added tying them to the preexisting aluminum table at the center of the main coil structure. The supports were lifted from below by a jack and checked by a digital level to ensure they were horizontal, then fastened in place.

Calibration Technique

Prior to the magnetic field alignment procedure a calibration of the magnetometer was necessary. The purpose of this process was to check the orthogonality of the sensor axes and to compare the readings with those of trusted equipment. The V-block was placed in a horizontal configuration, transverse to the beam direction, and the magnetometer, in its sled, was placed upon it such that the center of its sensor mass coincided with the future center of the ion chamber, which is at the geometric center of the coil array. As an initial step, the magnetometer was left static in this location and data were taken every few seconds for about five minutes. This data was used to examine the sensitivity of the device and the repeatability of the measurements taken with it. The fluctuations that were observed were on the order of a few microgauss, which was well within the required parameters of miligauss level sensitivity.

With the function of the magnetometer verified the current supplied to the primary holding coils was adjusted until the magnitude of the magnetic field produced by the main holding coils was at approximately 9 gauss. The orthogonality of the sensor axes was then checked by rotating the magnetometer through a series of 90 degree turns. If the axes are indeed orthogonal then the magnitude of the field should read the same along the three experimental axes regardless of the orientation of the magnetometer. Any difference in the readings between rotations indicates an angular separation between the sensor axes. These sensor misalignments were all found to be sub-miliradian in magnitude and changes were made to the data logging software to account for them in real time as new data were taken.

The alignment procedure was begun by characterizing the magnetic response to current change in each of the individual shim coils. This process ensures that each coil is functioning properly and gives a sense of scale and range for future adjustments. The current through the main holding coil was shut off and the current through a single shim coil was swept through a range of values while recording the resulting magnitude of the field along the affected axis. In this fashion, data for each shim coil were collected (Table 1) and used to generate the graphs of field strength versus current (Figure 20). The slopes of the resulting lines give a base point for further adjustments.

Alignment Procedure

All further measurements are complicated by the fact the sensors for individual axes do not inhabit a single point in space but are instead contained within a $4 \times 4 \times 2 \text{ cm}^3$ box. This results in at least two and quite possibly all three of the sensors being “off center” when a measurement is taken. As it is required that the field be wholly in the y-direction, the x and z components must be zero at the center of the coils. If adjustment to the shim coils is made without moving the magnetometer then those components will be zeroed at spatially separate locations which will cause small gradients to exist. To account for this asymmetry in sensor placement every measurement is made twice, with the magnetometer reflected about a single axis between measurements. If the field were uniform the difference in magnitude between two consecutive measurements would be zero, if this is not the case the current through the shim coils must be adjusted. This method is advantageous as it simultaneously allows for the minimization of the gradients and alleviates the need to reposition the magnetometer for measurements of each axis. Measurements were taken in this

Table 1. Data indicating the magnetic response to current change for individual shim coils.

Left Shim (A)	Bx (G)	Right Shim (A)	Bx (G)
0.11	0.05341	0.2	0.04543
0.21	0.04277	0.3	0.03622
0.31	0.032428	0.4	0.02686
0.41	0.022025	0.5	0.01749
0.511	0.011285	0.6	0.00763
0.611	0.0011507	0.7	0.00169
Back Shim (A)	Bz (G)	Front Shim (A)	Bz (G)
0.05	-0.01625	0.5	-0.0313
0.15	-0.01941	0.6	-0.03466
0.25	-0.02249	0.7	-0.03789
0.35	-0.02573	0.8	-0.04126
0.45	-0.02887	0.9	-0.04458
0.55	-0.03198	1	-0.04782

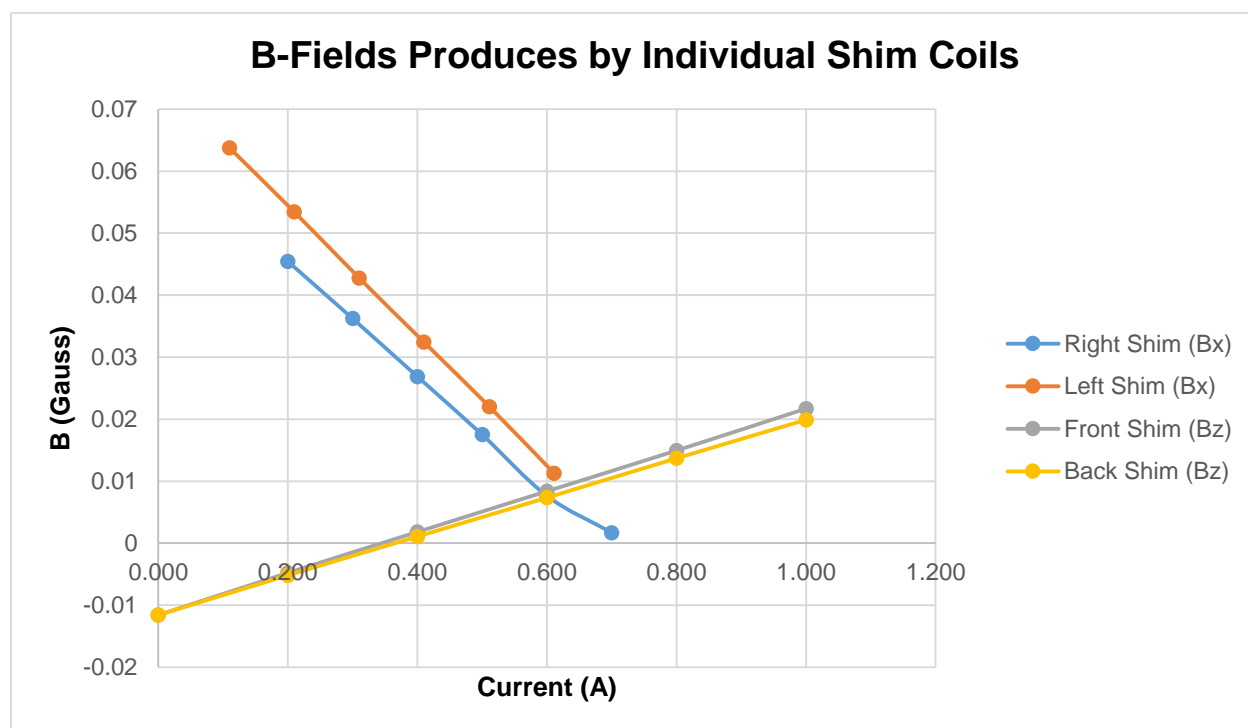


Figure 20. A graph of the above data. The slopes of the lines were used as a basis for further adjustments.

fashion and adjustments to the current through the shim coils periodically made until settings were found that resulted in acceptably small values of the differences in magnitude of the magnetic field in both the x and z-directions. These data are summarized in Table 2 and Table 3.

Due to the construction and placement of the coils, distortions in the shape of the field are more pronounced at the edges than at the center. Though preceding step acts to minimize the gradients and make the shape of the field as uniform as possible they must still be measured along the flight path of the neutrons to ensure they are within specified limits. With the V-block still in its transverse configuration, readings were taken at 10cm intervals along the x-axis. From this data the gradients dB_x/dx , dB_y/dx , and dB_z/dx were approximated. The V-block was then moved to a longitudinal configuration along the z-axis, re-leveled, and readings were taken at 10cm intervals from the beam guide to just past the ion chamber location. From this data the gradients dB_x/dz , dB_y/dz , and dB_z/dz were approximated. This same procedure was repeated four more times along the longitudinal axis with the V-block moved to locations 10cm off center above, below, left, and right of the z-axis. Example results are summarized in Table 4, Table 5, Table 6, Table 7, Figure 21, and Figure 22.

A possible source of perturbation was identified in a 30 ton gantry crane that services the beam lines on the north half of the SNS facility. It is an extremely massive steel I-beam which is capable of moving directly over the experiment hall and does so without warning. If significant coupling were to occur between this crane and the holding

Table 2. Data results from adjustment of left/right shim coil pair. Here, ΔB_x represents the difference between two consecutive measurements following a current adjustment. The shaded row reflects the current that was chosen for the final settings.

Left Shim (A)	Right Shim (A)	B _x (G)	B' _x (G)	ΔB_x (G)
0.21	0.5	0.00607	0.02338	0.01731
0.193	0.483	0.003608	0.026566	0.022958
0.226	0.516	0.011036	0.0202	0.009164
0.236	0.526	0.01206	0.018539	0.006479
0.256	0.546	0.01608	0.014723	0.001357
0.246	0.536	0.01417	0.01669	0.00252
0.25	0.54	0.014736	0.01612	0.001384
0.253	0.543	0.01589	0.015568	0.000322
0.252	0.542	0.015601	0.016277	0.000676

Table 3. Data results from adjustment of front/back shim coil pair. Here, ΔB_z represents the difference between two consecutive measurements following a current adjustment. The shaded row reflects the current that was chosen for the final settings.

Back Shim (A)	Front Shim (A)	B _z (G)	B' _z (G)	ΔB_z (G)
0.1	0.1	0.005352	0.009007	0.0036549
0.15	0.15	0.003028	0.01185	0.0148783
0.05	0.05	0.007669	0.004685	0.0029845
0.073	0.073	0.003857	0.006276	0.0024189
0.062	0.062	0.009497	0.006144	0.0033534
0.065	0.065	0.004766	0.007649	0.002883
0.068	0.068	0.009619	0.009082	0.0005365

Table 4. The magnetic field through the center along the x-axis, transverse to beam direction and gravity.

X(cm)	B _x	B _y	B _z
-20	0.013055	9.009215	0.017068
-10	0.01454	9.01156	0.016635
0	0.014364	9.018415	0.015509
10	0.011055	9.032481	0.014667
20	0.000707	9.046708	0.015856

Table 5. Gradients approximated from the field data along the x-axis.

X (cm)	$\Delta B_x/\Delta x$ (G/cm)	$\Delta B_y/\Delta x$ (G/cm)	$\Delta B_z/\Delta x$ (G/cm)
-15	0.000148416	0.00023449	-4.3273E-05
-5	-1.75238E-05	0.00068557	-0.000112653
5	-0.000330925	0.00140655	-8.41617E-05
15	-0.001034856	0.00142276	0.000118852

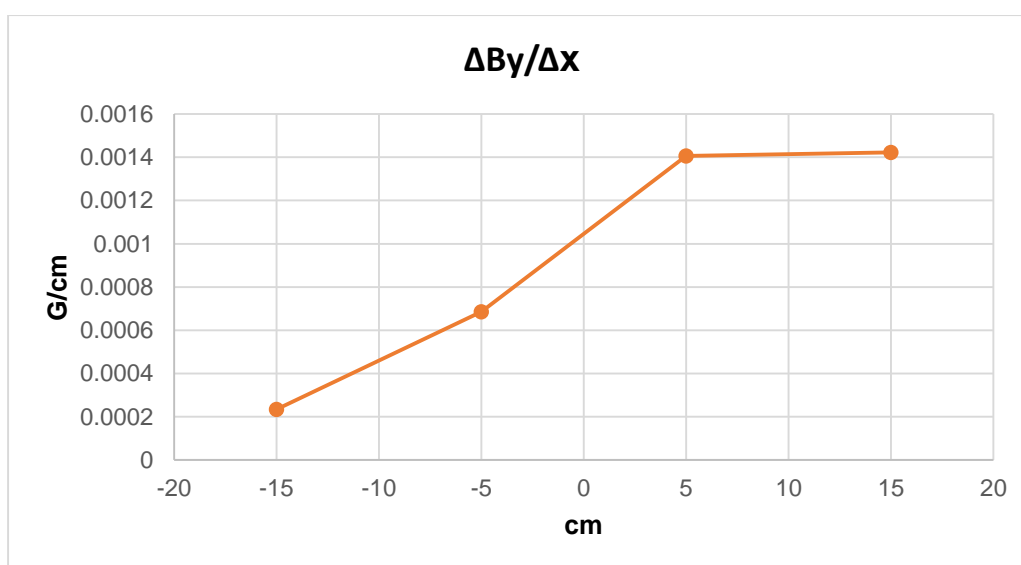


Figure 21. An example graph of the above gradient approximations.

Table 6. The magnetic field through the center along the z-axis.

cm	B _x (G)	B _y (G)	B _z (G)
-110	0.041672	9.215818	-0.01679
-100	0.043069	9.198932	-0.01951
-90	0.040876	9.156596	-0.01755
-80	0.039266	9.118819	-0.01614
-70	0.038371	9.091835	-0.01411
-60	0.020996	9.070815	-0.0088
-50	0.01441	9.055095	-0.00387
-40	0.011149	9.043231	0.004983
-30	0.013401	9.03363	0.012626

Table 6. (continued)

cm	Bx (G)	By (G)	Bz (G)
-20	0.005685	9.026573	0.020713
-10	-0.00162	9.021714	0.030534
0	-0.00054	9.018519	0.040071
10	-0.00175	9.017251	0.049156
20	-0.0114	9.017979	0.063545
30	-0.01132	9.020552	0.075922
40	-0.01112	9.024997	0.085218

Table 7. Gradients approximated from the field data along the z-axis.

cm	$\Delta B_x/\Delta z$ (G/cm)	$\Delta B_y/\Delta z$ (G/cm)	$\Delta B_z/\Delta z$ (G/cm)
-105	-0.000139713	0.0016886	0.000272036
-95	0.000219226	0.0042336	-0.000195742
-85	0.000161052	0.00377762	-0.000140429
-75	8.95262E-05	0.00269842	-0.00020361
-65	0.001737475	0.00210202	-0.000530958
-55	0.000658631	0.00157201	-0.000492811
-45	0.000326037	0.00118637	-0.000885367
-35	-0.000225186	0.00096011	-0.00076437
-25	0.000771642	0.00070572	-0.000808716
-15	0.000730634	0.0004859	-0.000982046
-5	-0.00010848	0.00031948	-0.000953674
5	0.000120878	0.00012684	-0.000908494
15	0.000965357	-7.284E-05	-0.001438975
25	-8.1062E-06	-0.00025725	-0.001237631
35	-1.94311E-05	-0.00044453	-0.000929594
45	0.000577211	-0.00063968	-0.001188755

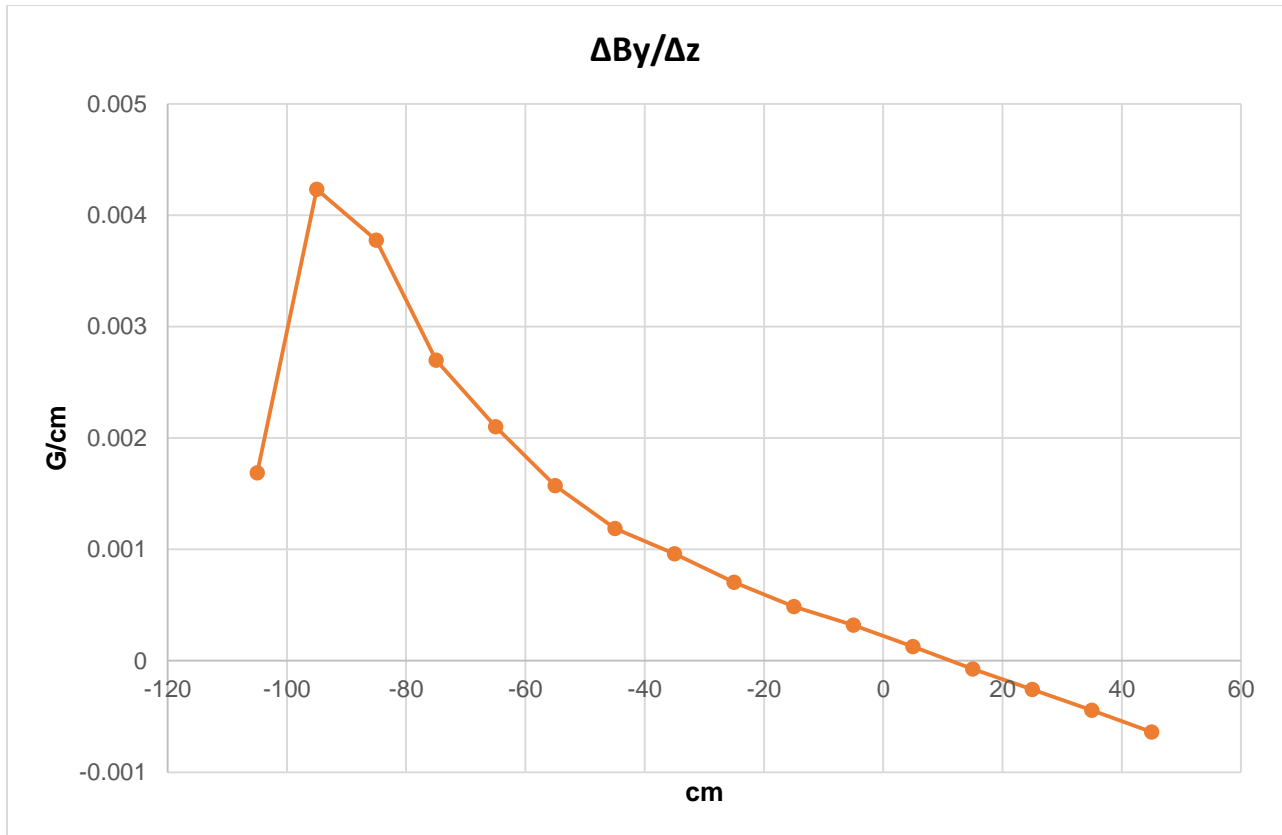


Figure 22. An example graph of the above gradient approximations.

field steps would need to be taken to either stop data collection while it was over head or account for it during analysis. The Magnetometer was placed back on its sled and repositioned at the center of the coil array. The crane was then translated at a constant velocity from one end of its track to another, crossing the experiment hall in the process. Magnetic field data were taken every several seconds for the duration of the cranes transit and it was found that, while there was some coupling, the change in the magnitude of the field was not significant enough to warrant extra measures. This data is summarized in Figure 23, Figure 24, and Figure 25.

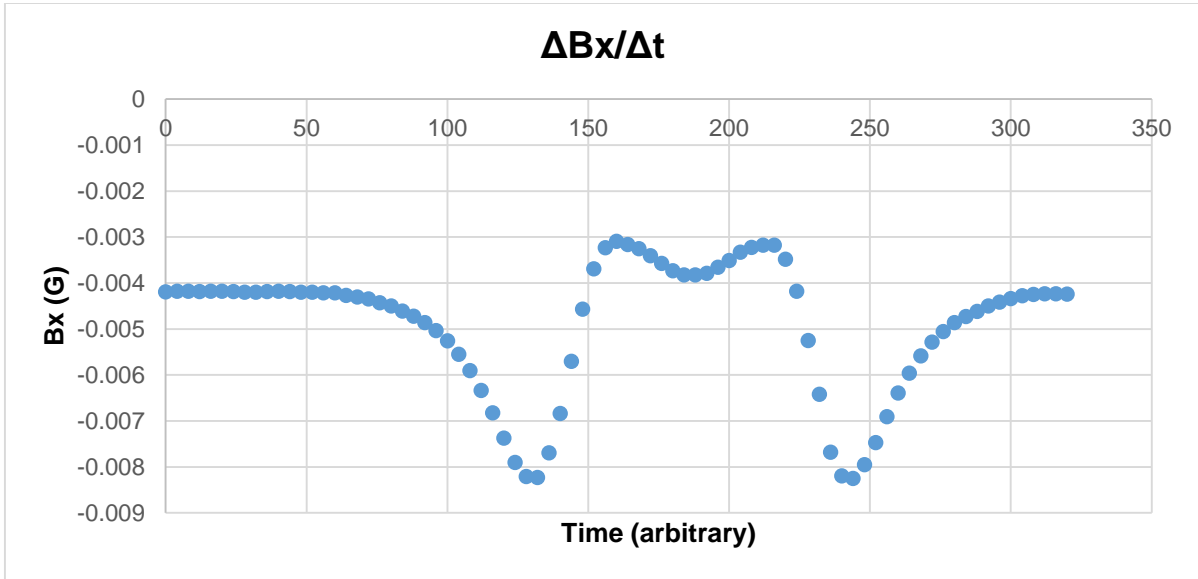


Figure 23. The change in B_x during the transit of the crane.

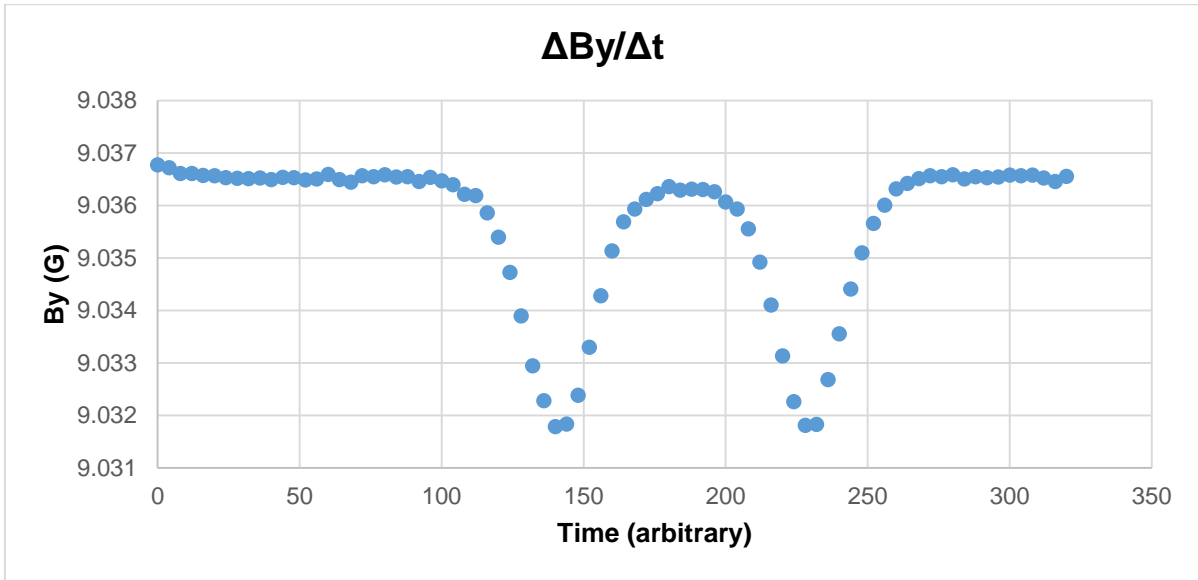


Figure 24. The change in B_y during the transit of the crane.

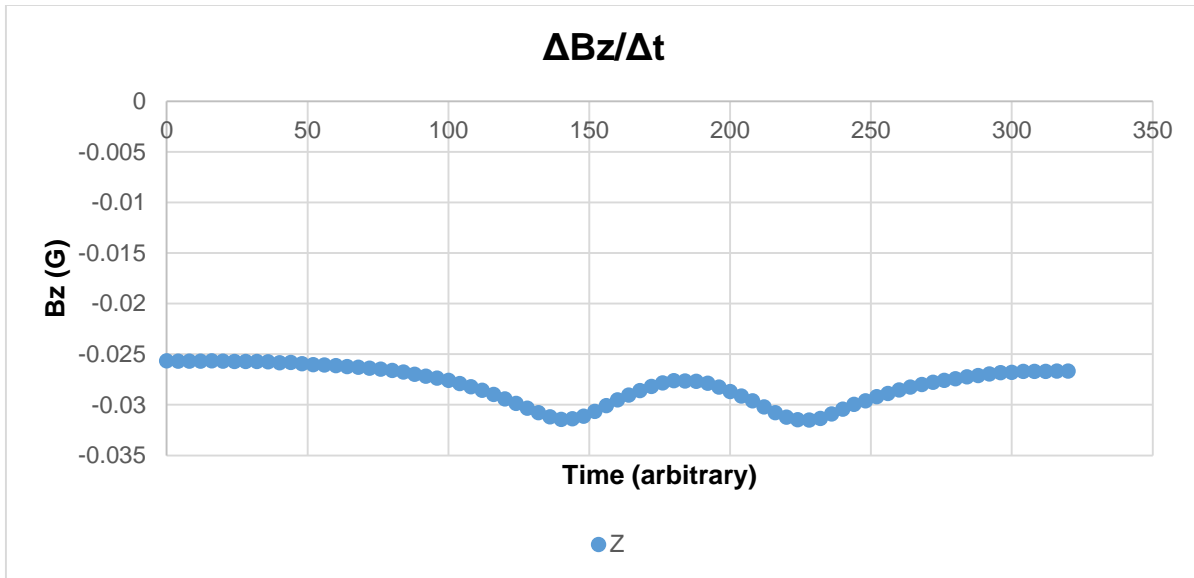


Figure 25. The change in B_z during the transit of the crane.

Once the gradients were shown to be acceptably small and the data from the transit of the crane was accounted for the magnetometer was removed from its sled and placed upon a stand such that it coincided with the future center of the RFSR. A final adjustment was made to the main holding field to increase the magnitude so that it had a value 9.13 Gauss. This is to accommodate the spin rotator which is a resonant circuit that is tuned to a particular frequency which the magnitude of the field must match. It should be noted that this adjustment produces minimal changes to the gradients.

Beam Scanning

In order to achieve appropriate placement of the primary components it is necessary to map the profile of the neutron beam and locate its centroid. This allows for ideal placement of components in the zone of greatest neutron flux. Sets of coupled translation tables (one that moves along the x-axis and one along the y-axis) equipped

with computer controlled stepper motors were inserted into the apparatus. One table from each set was fitted with a special alignment arm which doubles as a platform for a neutron detector. The tables were placed, with one set as close to the beam guide as possible and the other set as far away as possible, near the beam stop. Since the tables will be removed at the end of the following procedure there was no need to measure their positions relative to the support frame, save to ensure that they were perpendicular to the presumed beam direction. It is however necessary the tables be given an arbitrary origin from which to step. A location was chosen well outside of the beam profile so that the entirety of the beam profile could be scanned.

With the beam on, the tables were programmed to raster back and forth in a grid like fashion over the beam space pausing every 1cm to take a voltage reading from the beam scanner, which is directly proportionate to neutron intensity. From this data, the beam centroid was located by method of geometric decomposition.

$$\bar{X} = \frac{\sum_{n=1}^{N_x} V_n x_n}{\sum_{n=1}^{N_x} V_n} \qquad \bar{Y} = \frac{\sum_{n=1}^{N_y} V_n y_n}{\sum_{n=1}^{N_y} V_n}$$

Where \bar{X} and \bar{Y} are the x and y coordinates of the centroid, V_n is the voltage reading from the beam monitor at coordinates (x_n, y_n) , and the quantities N_x and N_y are the total number of data points taken. A line passing through both centroids determines the primary experimental axis. 2D and 3D graphs of both the upstream and downstream scans are shown in Figure 26, Figure 27, Figure 28, and Figure 29.

2D Graph

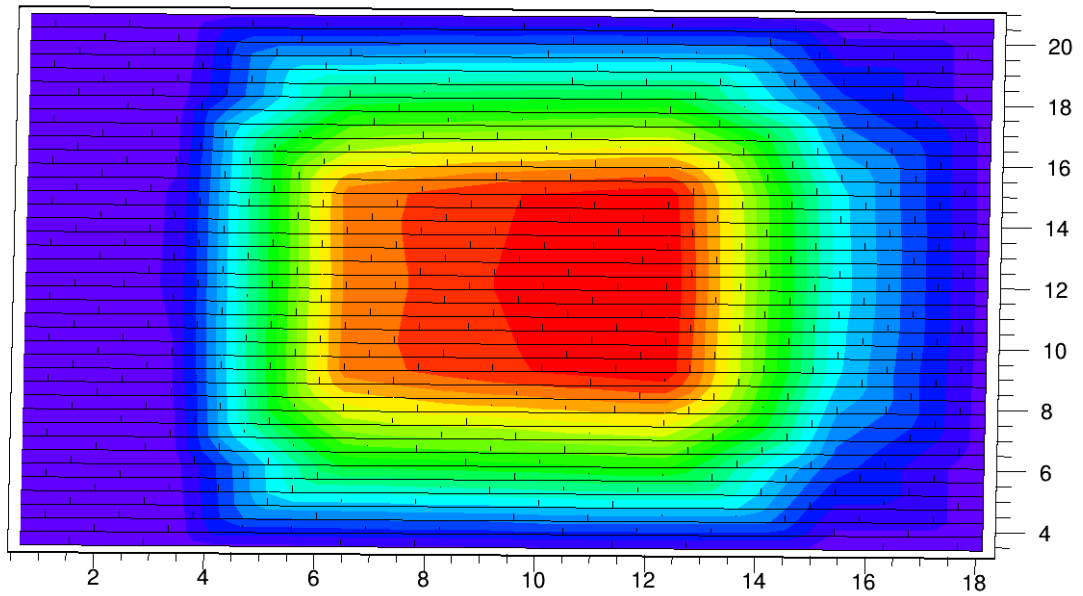


Figure 26. 2D scan of the upstream beam profile. The colors represent the magnitude of the voltage read from the scanner. Figure courtesy of Md. Kabir.

3D Graph

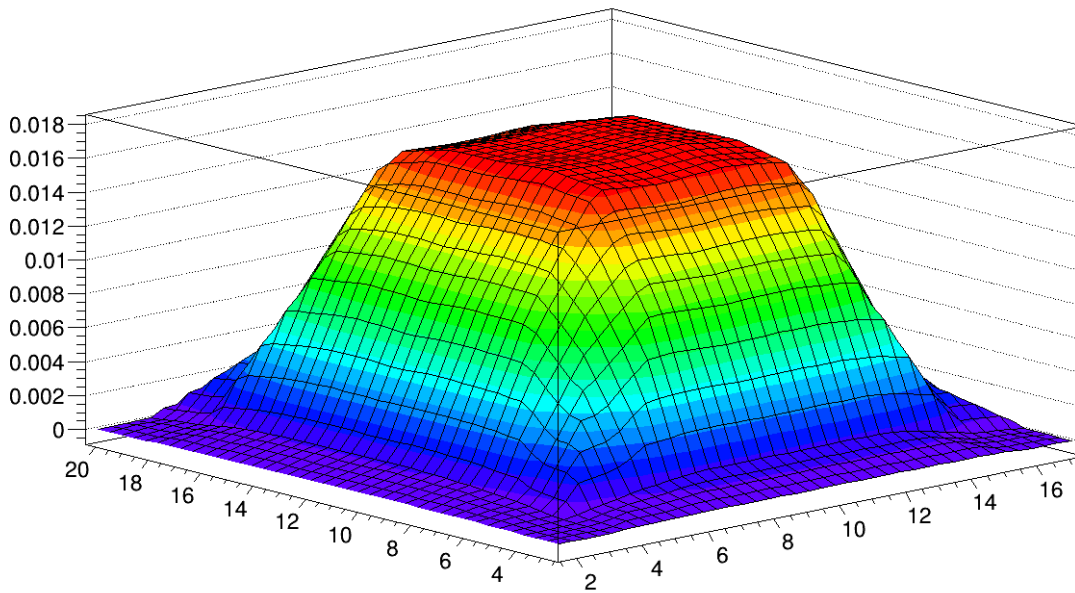


Figure 27. 3D image of the upstream data where the vertical axis (z) is voltage. Figure courtesy of Md. Kabir.

2D Graph

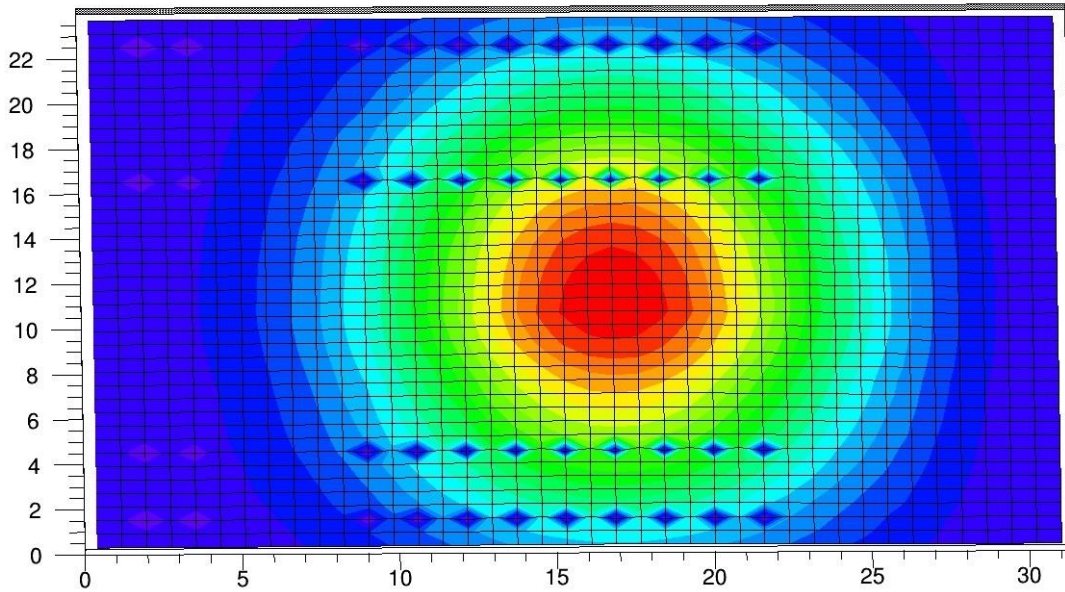


Figure 28. . 2D scan of the downstream beam profile. The colors represent the magnitude of the voltage read from the scanner. Figure courtesy of Md. Kabir.

3D Graph

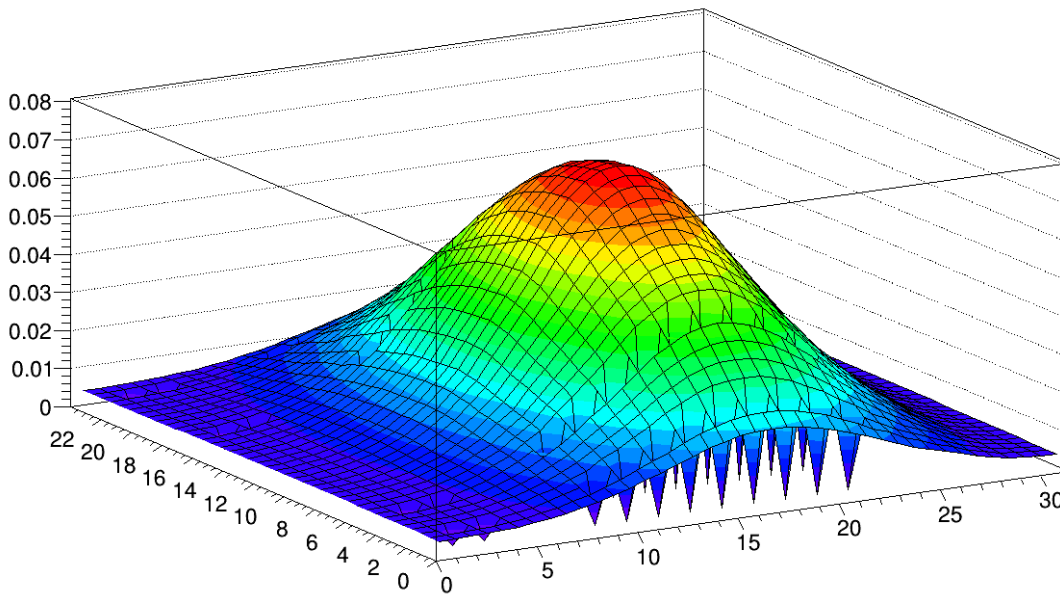
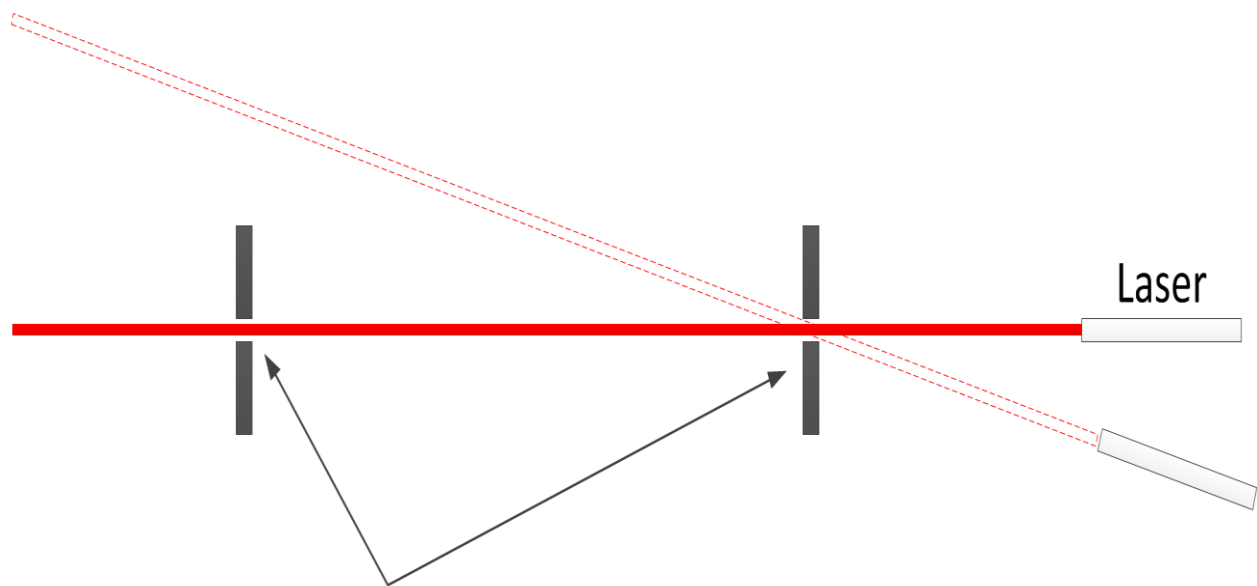


Figure 29. 3D image of the downstream data where the vertical axis (z) is voltage. Figure courtesy of Md. Kabir.

Once the centroid was located both sets of tables were displaced, in x and y directions, so that specially machined alignment holes in the armatures were coincident with the centroid. A laser attached to a kinematic mount was installed past the final set of tables, within the beam stop. This laser's position was then adjusted so that the beam passed precisely through the two alignment holes, and thusly along the beam axis as defined by the two centroids. An image of this process is shown in Figure 30. With the laser now defining the experimental axis the translation tables, which were no longer necessary, were removed to make way for the installation of the primary components.



Holes in xy-scanner apparatus defining beam centroid

Figure 30. As seen above, if the alignment laser is even slightly misaligned it will fail to shine through both alignment holes. Figure courtesy of Chris Hayes.

3D Modeling

At the time of the removal of the NPDGamma experiment from the experiment hall the $n^3\text{He}$ experiment was not yet ready for installation. While the primary components such as the RFSR and ion chamber were nearing completion, several minor components and structural framing had yet to be designed or constructed. To facilitate rapid development of these minor components and to ensure their proper fit and alignment, work was begun on a high resolution 3-D computer model. Though models of many of the components as well as the experiment hall itself were already in existence, nowhere was there available a comprehensive model in a single format.

The model was constructed using Autodesk Inventor 2015 over the period of several months. New renderings of the experiment hall and existing components were created based upon exhaustive physical measurements and portions of previous models were incorporated into the new model as well. As new components were designed they could be tested for fitment and alignment within the model eliminating the necessity of repeated physical installations and allowing for more rapid integration times.

The final model consists of over 300 individual 3-D parts files and over 1000 2-D drawings. In addition to being highly accurate, appropriate degrees of freedom and range of motion were incorporated for movable components, allowing for the visualization of various configuration changes as well as the testing of component/beam alignment procedures. The accuracy of this model allowed for near perfect initial placement of both the RFSF and ion chamber and very little adjustment was required during the final physical alignment.

Spin Rotator Installation and Alignment

The spin rotator was set upon an adjustable mount and placed closest to the beam guide (Figure 31). Due to the homogeneity of the field inside the spin rotator it is relatively insensitive to small misalignments in both the x and y directions. Its placement in the z direction was determined by the magnetic field set earlier. To remove angular deviations of the spin rotator from the beam axis a system of mirrors was devised to work in tandem with the alignment laser. A specially made steel plate was attached flush with the downstream face of the spin rotator. To this plate was attached a magnetically backed alignment mirror, constructed so that its mirrored face is parallel to its magnetic face. With the mirror attached, the position of the spin flipper was manually adjusted so the laser reflecting off the mirror was returned along the same path. To adjust the roll of the device a digital protractor was set atop the housing which was then rotated until it read zero.

Four Jaw Collimator Installation and Alignment

The four jaw collimator was installed next (Figure 32). The construction of this device is such that its overall position is automatically aligned upon installation. A simple alignment was required to determine the zero positions, with respect to the beam, of the two sets of doors. The doors were closed as pairs and the pairs were then translated until the alignment laser was split evenly by the seam between the two doors.

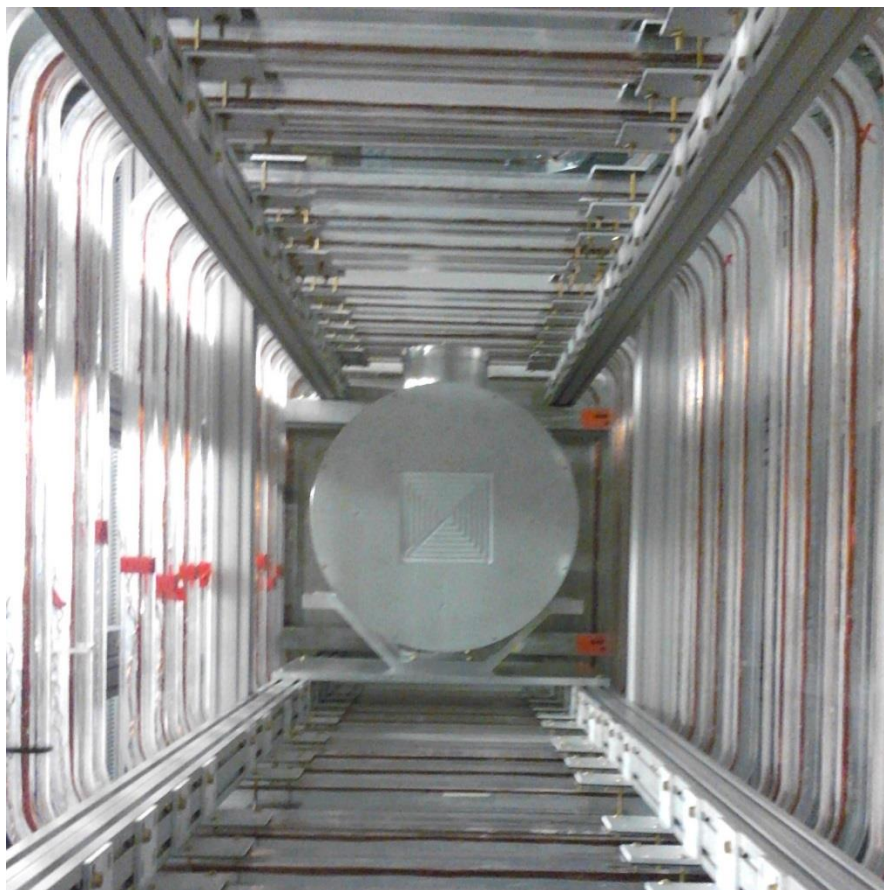


Figure 31. The spin rotator installed at the upstream side of the experiment.



Figure 32. The four-jaw collimator installed in front of the spin rotator. The ion chamber mount is visible in the foreground.

Ion Chamber Installation and Alignment

A large portion of the funding for this experiment was utilized in the construction of the ion chamber. It is a precision piece of equipment and to maintain its function it is important that it be handled with great care to avoid potential damage to its internal components. In addition, it is fairly heavy (over 80 lbs.) making it difficult and cumbersome to move in the tight quarters of the experiment hall. As such, a lift plan was devised to facilitate its safe insertion into the support frame.

A system of ropes and locking pulleys was devised that would allow the ion chamber to be hoisted from outside the support frame and then slowly translated along the longitudinal frame rails before being lowered onto its kinematic mount. Specially designed nylon rope stays were attached to the front and back of the ion chamber housing to facilitate the attachment of the rope and its free movement about the circumference. Nylon sliders were inserted into the upper longitudinal supports to carry the ropes and allow them to translate along the supports. On one side, the slides were fitted with simple carabineers to which the ropes were affixed and on the other they were fitted with progress capture pulleys that allow the rope to be easily drawn in one direction, corresponding to raising the ion chamber, but automatically lock if the rope is drawn the opposite direction, or dropped. The locks on the pulleys can be opened to allow for controlled descent.

To install the ion chamber, it was placed on a rolling cart with its beam axis parallel to gravity and positioned on the downstream side of the support frame. The support ropes were threaded through the rope stays and the chamber was slowly hoisted and rotated into its proper orientation. When the appropriate height was reached

to clear the support members the chamber was slowly towed to a location directly above its mount and lowered into place. This process is shown in Figure 33.

Prior to the installation of the chamber and its mount, the pair were pre-aligned. With the mount sitting on a fairly level lab table, the chamber was placed upon it and the mount adjusted to its anticipated position, drawn from the 3D model, in order to facilitate a more rapid alignment once installed (Figure 34).

Once the chamber was lowered into place the alignment procedure, utilizing the specially built kinematic mount, was begun. As the threaded rods, used to adjust both the angle and position of the chamber, are not orthogonal, adjustments made at any of the four tend to generate motions along/about multiple axes. This is further complicated by the free rolling nature of spherical contacts which, with the exclusion of the one in the conical recess, allow the chamber to have variable points of contact with the mount. To overcome these complications, a method was devised in which the chamber could be aligned by repeating an ordered sequence of adjustments and reducing the magnitude of the adjustments with each iteration.

Prior to adjustment, a reference mark (crosshairs) was placed at the center of the downstream face of the target chamber. This mark, when used with the alignment laser, allows for a coarse alignment by simply adjusting the mount until the laser and mark approximately coincide. The horizontal position of the chamber is controlled by the placement of the mount upon its support table hence it is this positioning that is the first to be dealt with. The mount itself is designed so that it will have the proper angular and longitudinal alignment upon installation, leaving only its transverse position to be



Figure 33. The ion chamber being hoisted into place. Note the progress capture pulley (orange). Photo courtesy of Jack Thomison.

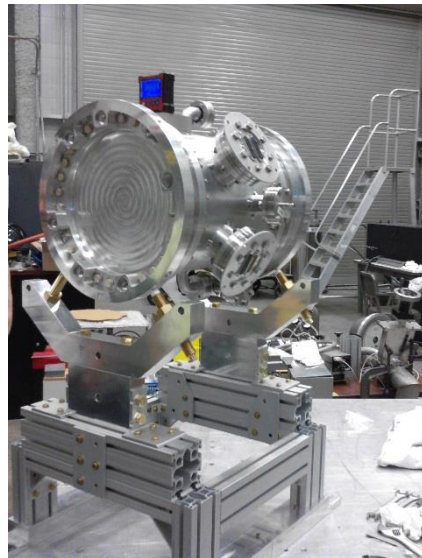


Figure 34. The pre-alignment of the ion chamber. The digital protractor which was used to level the chamber can be seen perched on top.

adjusted once the chamber is placed on it. This horizontal alignment is a simple matter of translating the mount/chamber combination along the x-axis until the beam from the alignment laser coincides with the vertical cross hair. Once this was complete, the mount was fastened in place and will not be moved for the duration of the experiment. The vertical position of the chamber is controlled by simultaneous adjustments of all four threaded rods which were turned until the laser beam coincided with the horizontal crosshair. Once coarse alignment was completed, a steel plate was fastened to the downstream face of the chamber and the same alignment mirror used to align the spin rotator was magnetically attached to the center. As with the spin rotator, alignment was achieved by reflecting the laser back to its point of origin.

For the fine alignment, the first step was to adjust the yaw (misalignment in the xz-plane and about the y-axis). This was achieved by adjusting the threaded rods in crosswise pairs, upstream-beam left and downstream-beam right for example. This primarily generates rotation about the y-axis and is continued until displacement of the reflected laser beam to the left or right of its point of origin is zero. Next the pitch (misalignments in the yz-plane about the x axis) was corrected. By simultaneously making adjustments of the same magnitude to upstream or downstream pairs of threaded rods, rotations about the x-axis can be produced. This process was continued until up or down displacements of the laser from its point of origin are zero.

The horizontal position was then corrected. The roll of the chamber (rotations about the z-axis) was then corrected. Adjustment of roll may be achieved by either adjusting left or right pairs individually or by adjusting one pair in one direction and the other pair in the opposite direction. The second method was found to give better results

as it minimizes unwanted horizontal and vertical displacements. The rotational alignment procedure in all cases, both coarse and fine, was facilitated by a digital protractor placed upon a flat surface atop the chamber housing.

With pitch, roll, and yaw adjusted, the alignment mirror and steel backing plate were removed to reveal the reference crosshairs. Due to the aforementioned non-orthogonality of the kinematic mount, the preceding angular alignment procedures will have produced minor horizontal and vertical displacements which needed to be accounted for. The vertical position was adjusted as previously described. The horizontal position of the chamber was primarily achieved during the installation of the mount itself but minor adjustments can be made by adjusting beam left pairs of rods in one direction while simultaneously adjusting beam right pairs in the opposite direction or by adjusting left and right pairs individually. This procedure can only be used for very small horizontal adjustments as it will always produce undesired rotations. The first method will result in less roll of the chamber but either case will result in unwanted rotations.

This ordered procedure of adjusting yaw, pitch, roll, vertical position, and horizontal position was repeated until the desired alignment requirements were met. After each iteration the magnitude of the adjustments required to realign the chamber were greatly reduced. A series of three iterations was sufficient to achieve the desired accuracy. A model typifying this process is shown in Figure 35.

All of the above alignment procedures were measured with respect to the chamber housing but the most important alignment is with respect to the wire planes

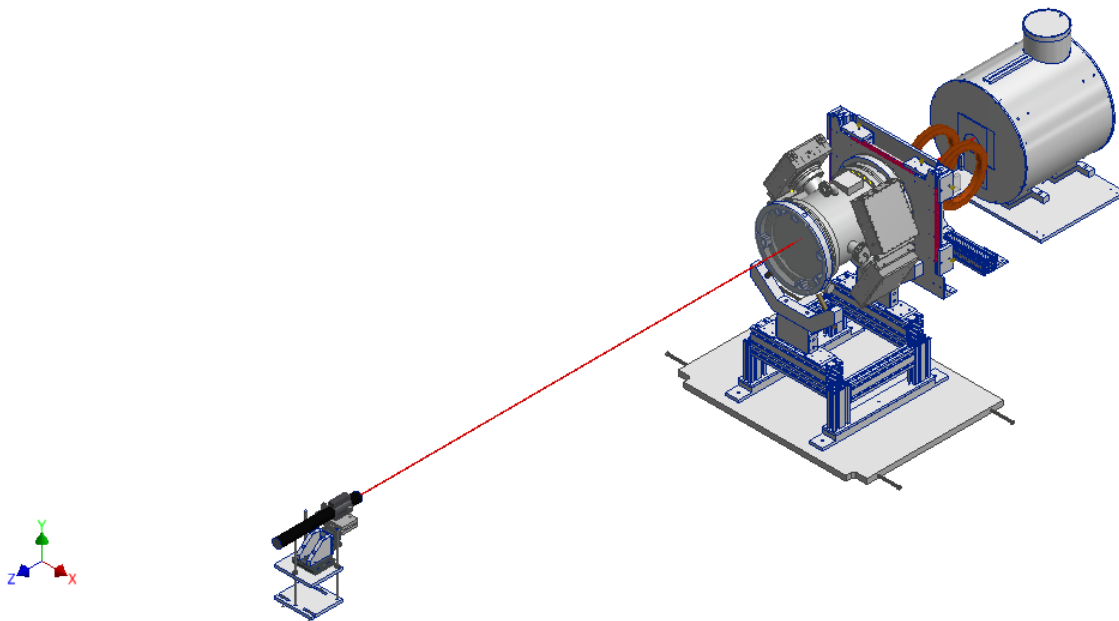


Figure 35. This model typifies the laser alignment of the RFSR, four-jaw collimator, and ion chamber. Only when properly aligned will the laser beam be reflected back precisely to its point of origin.

within the ion chamber. Since, at the time of installation, the chamber had already been filled with expensive and difficult to procure ^3He gas it was impossible to see the wire planes or to directly measure their orientation. As a safety check and backup to our procedures, the ORNL survey and alignment team made a set of independent measurements.

Using a suite of sophisticated surveying equipment and software a series of measurements was made relating the position and orientation of the wire planes to points on the exterior of the housing. These measurements were made prior to the chamber being filled and sealed. A series of alignment markers, called fiducials, were glued to multiple locations on the housing, and their positions relative to one another measured and recorded in a 3D model. The wire planes were then surveyed and their

positions and orientations were incorporated into the model. As the internal components of the chamber are fixed with respect to the housing this model allows knowledge of the exact locations of the wire planes by simply resurveying the fiducials. Once the alignment procedure was completed, the survey and alignment team was invited back to confirm the quality of our installation. The data they received revealed no alignment issues of large enough magnitude to warrant any further adjustment and with completion of their check, the experiment was deemed ready for commissioning runs.

CHAPTER 5: CONFIRMATION OF ALIGNMENT

Commissioning.

Before the experiment is ready to run full time it was subjected to a commissioning phase, during which the safety and function of the experiment and its components were tested. Early polarimetry results were obtained which give evidence that the alignment of the magnetic field is satisfactory and results from tests on the ion chamber lead to similar confidence in its alignment. This evidence, coupled with the checks by the ORNL survey and alignment team, gives us sufficient confidence to begin running the experiment full time.

Spin Rotator Efficiency

It is possible to invert the net polarization of the ^3He spin filter, using the AFP coils, and it may thus be used to transmit or absorb neutrons of either spin state. So, in addition to monitoring the polarization of the neutron beam itself, the polarimetry apparatus may also be used to measure the efficiency of the RFSR. This efficiency is calculated to a high degree of accuracy by comparing the amount of transmitted neutrons from the RFSR while it is on to those transmitted while it is off. After the RFSR was tuned by making some small adjustments to the main holding field, efficiencies were obtained that were greater than 99%. Since the RFSR was aligned with gravity this demonstrates that the alignment of the magnetic field with the local gravitational field is extremely precise.

Ion Chamber Alignment Check

As previously mentioned, the alignment of the ion chamber and its internal wire planes was checked by a survey and alignment team. It should be noted that both our initial alignment and their check were performed with respect to gravity. However, in light of the results of the polarimetry measurements, the quality of the alignment was verified. The most important issue for the ion chamber is that it be at the appropriate angle with respect to the spin of the neutrons. The polarimetry results demonstrate the strong correlation between the magnetic field and gravity and, by extension, between the neutron spin and gravity.

Additional confidence can be gleaned from another series of tests that were performed on the ion chamber during commissioning. In order to verify the function of the individual wires within the chamber a slit test was performed. During part of this test, the four jaw collimator was arranged such that the vertical doors were opened to the full width of the chamber and the horizontal doors were closed to an opening size of slightly less than 0.5cm, a distance roughly corresponding to the inter-wire spacing inside the chamber. This half centimeter slit was then translated to lie over each wire in turn and intensity data were taken with the beam on and the beam off. When the intensity data were graphed the difference between the two sets of data were found to be markedly different, which is a strong indication that the chamber is functioning properly. The final proof of the precision of the alignment will be in the examination of the final data once the experiment is complete.

Concluding Remarks

The construction and commissioning phases of the $n^3\text{He}$ experiment are complete and there is sufficient evidence to show that the alignment procedures were successful and to support the decision to move to full time data collection. The experiment is currently running at the SNS and is expected to conclude data collection in December of 2015 after which some time will be spent in analyzing and interpreting the data before the results are published.

Works Cited

- [1] J. D. B. H. Bertrand Desplanques, Unified Treatment of the parity violating nuclear force, *Annals of Physics* 124(2):449-495, 1980.
- [2] C. Hayes, Spin Flipper and Neutron Polarimetry for the $n^3\text{He}$ Experiment, University of Tennessee, Department of Physics and Astronomy, 2014.
- [3] How The Spallation Neutron Source Works,
<http://neutrons2.ornl.gov/facilities/SNS/works.shtml>, 2014.
- [4] M. J. Dadras, Polarimetry Studies for the NPDGamma Experiment at the SNS., Master's Thesis, University of Tennessee, Department of Physics and Astronomy, 2009.
- [5] <http://neutrons2.ornl.gov/facilities/SNS/works.shtml>, ORNL, 2014.

Vita

Eric Plemons was born in Fort Riley, Kansas to a military family and moved frequently before settling down in Maryville, Tennessee where he attended Alcoa High School. He began attending the University of Tennessee in 2009 and received a Bachelor's in Engineering Physics in 2012. After receiving his Bachelor's he entered the graduate program in the Department of Physics and Astronomy to pursue a Master's degree.